NANOMATERIALS DOPED THIN ORGANIC COATINGS FOR APPLICATION OF POWER TRANSMITION AND CABLE INDUSTRY

by

Hamdi Harun ARKAZ

A thesis submitted to
the Graduate Institute of Sciences and Engineering
of

Meliksah University
in partial fulfillment of the requirements for the degree of
Master of Science
in

Materials Science and Mechanical Engineering

August 2014

Kayseri, Turkey

This is to certify that I have read the thesis entitled “Nanomaterials Doped Thin Organic Coatings for Application of Power Transmition and Cable Industry" by Hamdi Harun ARKAZ and that in my opinion it is fully adequate, in scope and quality, as a thesis for the degree of Master of Science in Material Science and Mechanical Engineering, the Graduated Institute of Science and Engineering, Melikşah University.

Assoc. Prof. Mehmet HANÇER

Supervisor

I certify that this thesis satisfies all the requirements as a thesis for the degree of Master of Science.

Head of Department

Examining Committee Members

_____ (Signature)_____

_____ (Signature)_____

_____ (Signature)_____

It is approved that this thesis has been written in compliance with the formatting rules laid down by the Graduate Institute of Sciences and Engineering.

Director

August 2014

NANOMATERIALS DOPED THIN ORGANIC COATINGS FOR APPLICATION OF POWER TRANSMITION AND CABLE INDUSTRY

Hamdi Harun ARKAZ

M. S. Thesis – Materials Science and Mechanical Engineering

August 2014

Supervisor: Assoc. Prof. Mehmet HANÇER

ABSTRACT

High and medium voltage power transmission cables in the world and in Turkey are produced from steel-backed aluminum and aluminum alloy metal cables. As for the conductive materials, especially aluminum is preferred due to its high mechanical strength, low electrical resistance and lower cost. The internal steel core of the wire carries the load while the aluminum beams surrounding the core carries the electrical current. In another application, steel wire surrounding the polymeric core (polypropylene or hemp) of which oiled against metal corrosion is also used for carrying and towing the load. Aluminum conductor cable and steel wire rope products are often exposed to moisture, heat, wind, snow, ice and extreme environmental conditions during their service life.

As a result, the reduction in electrical conductivity due to loss of material (corrosion), audible noises interfering with transmission (broad band) and radio lines due to micro

arcs and in particular wire break offs, elongations and pole bending and collapses are in common.

The material properties changes dractically when size reduced to nano scale due to the increased volume to mass ratio at the surfaces and interfaces. In this work, opaque and wear resistant composite thin films reinforced with active material doped nano clay materials will be used to coat aluminum energy transfer cables and load bearing steel ropes for anti-corrosion and anti-icing purposes. Anti-corrosion and anti-icing nano composite coatings will be obtained with the dispersion of intercalated nano clays into the poly silicone matrix (Gelest HardSil or Dow 840). Then 10x10 cm sized aluminum metal plates will be dipped into poly silicon suspensions in order to produce robust thin films. The coated metal plates then will be heat cured at moderate temperatures (105oC) for 15 minutes in order for better adhesion to metal surface and cross linking as well. In this method, transparent coatings of 10-15 micron thick with high abrasion resistant will be achieved (Taber 500 500g CS10F cycle of 5% or better). This study is also supported by Ministry of Science, Industry and Technology in SANTEZ which its code is 1183.STZ.2012-1

Keywords: Aluminum cable, steel rope, corrosion, icing, nano composite, hydrophobic, wear, coating**.**

NANOMALZEME KATKILI İNCE ORGANİK KOMPOZİT KAPLAMALARIN ENERJİ NAKİL KABLOLARINDAVE HALAT SANAYİNDE KULLANILMASI

Hamdi Harun ARKAZ

Yüksek Lisans Tezi – Malzeme Bilimi ve Makina Mühendisliği

Ağustos 2014

Tez Yöneticisi: Doç. Dr. Mehmet HANÇER

ÖZ

Yüksek ve orta gerilim enerji nakil kabloları, dünyada ve Türkiye de çelik destekli alüminyum ve alüminyum alaşımlı metal kablolardan üretilmektedir. İletken malzeme olarak alüminyum, özellikle yüksek mekanik dayanım, düşük elektrik direnci ve ucuz olması nedeni ile tercih edilmektedir. İç kısımdaki (çekirdek) çelik halat mekanik yükleri taşırken, çelik halatı çevreleyen birkaç katmalı alüminyum demeti de elektrik akımını taşır. Bir diğer uygulama da ise korozyon önlemek amacı ile yağa batırılmış kendir (veya polipropilen) elyaf çekirdek etrafına sarılmış çelik halatlar yük taşıma ve çekme amacı ile kullanılmaktadır. Alüminyum iletken kablo ve çelik halat ürünleri, kullanımı sırasında sıklıkla nem, ısı, rüzgâr, kar, buz gibi çok değişken ve aşırı çevre şartlarına maruz kalmaktadır. Bunun sonucunda aşınmalara bağlı elektrik iletkenlik azalması, nakil hatlarından gelen duyulabilir seslerin radyo ve telefon hatlarında parazit yaratması,

(broad band interference) ve neme bağlı korozyon oluşumları gözlemlenmektedir. Ayrıca özellikle nakil hatları üzerinde oluşan buzlanmalara bağlı olarak kopmalar ve istenmeyen malzeme uzamalarına ve nakil direklerinin hasara (eğilme, çökme vb) uğramasına neden olmaktadır.

Aşınmaya dayanımı yüksek nano malzeme (partikül, lif vb) takviyeli yeni nesil ince kaplamalar ve kompozit malzemelerin özellikle son yıllarda kullanım alanları hızla artmıştır. Nano boyutlara inildiğinde artan yüzey alanı/hacim oranı malzemeyi daha aktif yaparak yüzey ve ara yüzeylerde daha farklı etkileşimlere neden olur. Bu çalışmada yüksek gerilim enerji nakil hatlarında kullanılan iletken alüminyum ve taşıma amaçlı kullanılan çelik halatların yüzeylerinde aşınmaya dayanıklı aktif nano kil içeren, korozyon ve buzlanmayı (hidrofobik) önleyici ince polimer nano kompozit kaplamaları üretilecektir. Nano kompozit kaplamalar, aktif madde içeren (anti-corrosion, anti-icing) tabakaları açılmış doğal nano killerin silikon tabanlı hidrofobik polisilikon bir reçinenin (Gelest Hard Sil, Dow chemical vb) solvent süspansiyonu içerisine disperse edilmesi ile elde edilecektir. Daha sonra alüminyum ve çelik halat yüzeyleri daldırma (dip coating) tekniği ile hareketli bir makara vasıtası ile süspansiyon içerisinden geçirilerek nano-kompozit kaplama uygulaması gerçekleştirilecektir. Kaplanan halatlar yine makaralar vasıtası ile bir ısı tünelinden geçirilerek 105 oC de 15 dakikada sertleştirilerek (curing) çapraz bağlama (cross-linking) gerçekleştirilecektir. Elde edilecek aktif katkı maddeli nano kompozit şeffaf kaplamalar 10-15 mikron kalınlıkta ve yüksek aşınma dayanımına (Taber 500 cycle 500g CS10F % 5 veya daha iyi) sahip olacaktır. Proje konu itibarı ile Tübitak tarafından belirlenmiş ve ülkemiz için ulusal öncelikli bilim konularından (UBTYS 2011-2016) olan nanoteknoloji alanındadır.

Anahtar Kelimeler: Alüminyum kablo, çelik halat, korozyon, buzlanma, aşınma, nano kompozit, hidrofob, kaplama

DEDICATION

to make the world a better place

ACKNOWLEDGMENT

I express sincere appreciation to Assoc. Prof. Mehmet HANÇER for his guidance and insight throughout the research.

Thanks go to other members of department of Materials Science and Engineering and ERNAM - Erciyes University Nanotechnology Research Center -

Special thanks for technical assistance to Mehmet TAŞ and İsmail KILIÇ are gratefully acknowledged.

I expressed my thanks and appreciation to my wife for their understanding, motivation and patience.

TABLE OF CONTENTS

LIST OF TABLES

TABLES

LIST OF FIGURES

FIGURE

CHAPTER 1

INTRODUCTION

1.1 SURFACE ENERGY AND SURFACE TENSION

The presence of an interface between two phases results in a change free energy compared to inside the materials. Two results of interface atoms/molecules effect equilibrium properties; the surface energy, γ (J/m2), and surface tension, γij (N/m). [1, 2] A distinction is made between the surface energy and the surface tension. The surface energy is the work necessary to form unit area of surface by a process if division: the surface tension is the tangential stress (force per unit length) in the surface layer; this stress must be balanced either by external forces or by volume stresses in the body. [3]

As Shuttleworth (1949) said; according to Millington (1945, 1947) the concept of the surface tension was introduced by Cabeo (1629) and was stated more explicitly by Segner (1751). Theories that explain the surface tensions of liquid in terms of molecular forces have been advanced by Young (1805), Laplace (1806), Poisssion (1830), Wortington (1884), Bakker (1928), Brown (1947) and Prandtl (1947). [3]

The concept of surface energy is more recent and was introduced by Gauss (1830). Reyleigh (1890) has shown that for the Laplace model of a liquid the surface tension and energy are numerically equal. Gibbs (1876) pointed out that for a solid they are not equal, and that the value of the surface tension in a particular crystal face can vary with direction. Recently Orowan (1950) and Nicolson (1950) have discussed the surface tensions of solids in detail, and Nicolson has calculated the surface tensions of some ionic crystals from the force constants of their ions. [3]

1.1.1 Surface Energy

The term of surface is commonly reserved for the boundary between a condensed phase (liquid or solid) and a gas or liquid with the term ‘interface’ being used to describe the junction of the two condensed phase.[4] The atoms at the surface of a condensed-phase material are in a very different environment compared to those atoms from its interior. [5] The molecules at the surface do not behave like other molecules on all sides of them and consequently they cohere much stronger to those directly associated with them on the surface.[4] Differences between the energies of atoms (or molecules) located at the surface and in the bulk manifest themselves as surface energy, γ. [5]

As shown Figure 1.1, the molecules in the inner layer are in the balance or the forces in a state of equilibrium between them and this will give zero force difference in all angles. The molecules on the surface are faced with an unbalanced force due to missing molecules on the surface. Net balance forces are created on the surface that results in surface energy. [4]

Consider a large one-component crystal in equilibrium with its vapor in a constant volume enclosure that is maintained at a constant temperature. If this crystal is divided into two parts by a plane whose indices are p and the two parts then separated, the free energy of the system increases by amount Ap x Fp, where Ap is the increase in surface area, and Fp is defined as the surface free energy per unit area. [3] If the cutting is done reversibly, then conservation of energy means that the energy consumed by cutting process will be equal to the energy inherent in the two new surfaces created. [6] Consequently, external work that is needed will equal the increase in total free energy of system. [3]

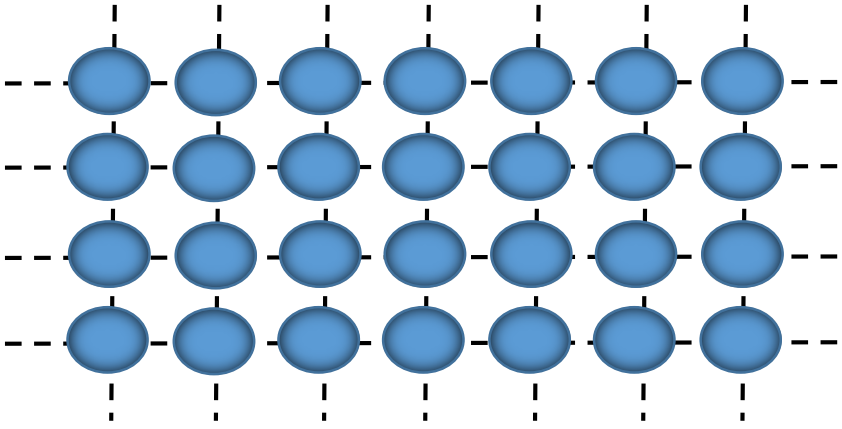

Figure 1. 1 Surface Energy, The result of the unbalanced forces on the surface atoms.

As shown on Figure.1.2, each molecule in the interior has six bonds to its neighbors whereas a surface molecule has only five. If the total bonding energy of a molecule in the bulk is E, a surface molecule will only be bound by 5/6 E. The missing binding energy corresponds to adding an extra positive energy 1/6 E for each surface molecule. As it is seen in the figure, missing binding energy will also increase at corner and edge. When a crystal is a large compared with atomic dimensions. It is possible to neglect the extra energies of edges and corners. The surface free energy is only a small correction to the total free energy of the system. For an isotropic material with a curved surface the surface free energy per unit area will be supposed independent of the curvature of the surface, in analogy with the neglect of the edge and corner energies of a crystal. [3]

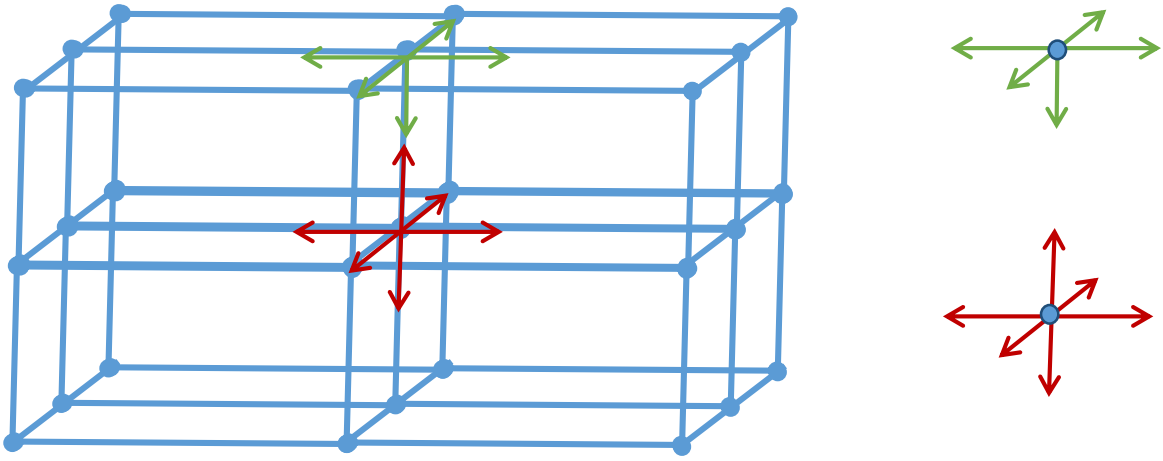

Figure 1. 2 Bonding of Interior and Surface Atoms of a Simple Cubic Structure

Basically, there are two parameters are needed to find the total free energy of a surface;

- The breaking of bonds on the surface – surface coordination number-
- The energy of one bond

For one- mole crystal structure, there are 0,5NA bonds form among them. Numbers of total bonds in one mole crystal are founded when 0,5NA multiply by coordination number, Z. The energy of one bond is written as;

$$\varepsilon = \frac{\Delta Hs}{0{,}5NA\ x\ Z} \tag{1.1}$$

where ΔHs is the molar enthalpy (evaporation enthalpy).

For the (100) plane in the simple cubic structure, total coordination number is 6 and surface coordination number is 3, which mean 3 missing bonds per atoms at surface. Total binding energy on surface at (100) plane is written as;

E (100) = (energy of one bond) x (number of missing bonds per atom)

$$= \varepsilon \times 3 = \frac{\Delta Hs}{0{,}5NA \; x \; 6} = \frac{\Delta Hs}{NA} \tag{1.2}$$

energy required per surface atoms.

The surface energy, γ, can be found as multiply by this value with ratio of number of surface atoms, Nsand surface area, as;

$$\gamma(100) = \frac{\Delta Hs}{NA} \; x \; \frac{Ns}{As} \tag{1.3}$$

According to system, most important parameters are "surface coordination number" and surface atom density. Because of this, not only structure but also plane system of surface is important for value of surface energy.

- For FCC crystal γ(110) > γ(100) > γ(111)
- For BCC Crystal γ(111) >γ (100) >γ(110)

Thermodynamically, the surface energy, γ, is interpreted as the increase in the Gibbs energy of the system when the area of the interface under consideration is increased reversibly by an infinitesimal amount dA at constant temperature (T), pressure (p) and composition (n) [2,5]. This can be expressed as;

$$\gamma = \left(\frac{\partial G}{\partial A}\right) T, p, n \tag{1.4}$$

The surface energy density associated with a liquid or solid interface against vacuum (or gas) is always positive because of the missing negative binding energy of the surface molecules. The positivity of the surface energy density guarantees that such interfaces seek towards the minimal area consistent with the other forces that may be at play, for example gravity. Small raindrops and air bubbles are for this reason nearly spherical. Larger falling rain drops are also shaped by viscous friction and air currents, giving them a more complicated shape.

Interfaces between solids and liquids or between liquids and liquids are not required to have positive interfacial energy density. The sign depends on the strength of

the cohesive forces holding molecules of a material together compared to the strength of the adhesive forces between the opposing molecules of the interfacing materials. The interface between a solid and liquid is normally not deformable, and a negative interfacial energy density has no dramatic effect. If on the other hand the interfacial energy density between two liquids is negative, a large amount of energy can be released by maximizing the area of the interface. Folding it like crumpled paper, the two fluids are mixed thoroughly instead of being kept separate. Fluids that readily mix with each other, such as alcohol and water, may be viewed as having negative interfacial energy density, although the concept is not particularly well-defined in this case. Immiscible fluids like oil and water must on the other hand have positive interfacial energy density which makes them seek towards minimal interface area with maximal smoothness.

1.1.2 Surface Tension

It has long been recognized that the surface tension need not to equal the surface energy for solids. However, it is well-known that surface tension is positive with numerical value equal to the surface energy for a liquid. [1] The molecules at the surface of a liquid are attracted into the body of the liquid because the attraction of underlying molecules is greater than the attraction by the vapor molecules on the other side of the surface. This inward attraction causes the surface to contract if it can and gives rise to a force in the plane of the surface. [7] Solids also have surface tensions, but it is hard to measure them. Crystals tend to form with faces with lowest surface tensions.

Figure 1. 3 The surface tension of water allows the water striders on the water without sinking [Max Westby-asknature.org]

Surface tension is a property that allows the surface of a liquid to behave somewhat as a trampoline does. When a person stands on a trampoline, the trampoline stretches downward a bit and, in so doing, exerts an upward elastic force on the person. This upward force balances the person's weight. The surface of the water behaves in a similar way. [8] In Figure 1.3, the feet of the insects create indentation on the water surface, because it can stride or walk on the surface just as a person can walk on a trampoline.

The surface tension of a liquid, γ, which measures the mechanical work required to stretch the surface (or interface) at fixed composition, must be balanced either by external forces or by volume stresses in the body. [2] Because of this, it is typically measured in dyne/cm or N/m or, since 1J = 1Nm, J/m^2. Basically, it is the force per unit length on the surface that opposes the expansion of the surface area. The most basic surface tension experiment, illustrated in Figure1.4, is a 2D version of a 3D experiment where the movable bar is pulled with fore F to expand a liquid film that is stretched like a soap-bubble film on a wire frame. [2, 7]

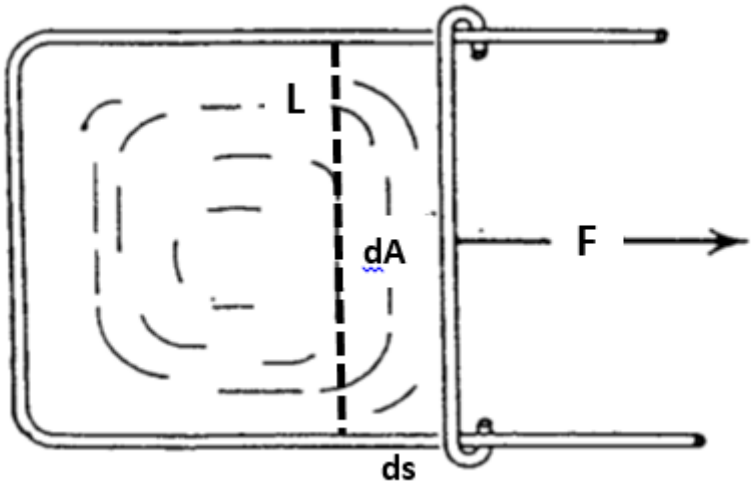

Figure 1. 4 Idealized experiment for the determination of the surface tension of a liquid.

Since the area increased by dA = L x ds, it takes an amount of work dW = γLds, from which the applied force orthogonally to the line is F = dW/ds = γL. In equilibrium, the applied normal force per unit of length, F/L = γ.

The surface tension of a liquid may be measured by a variety of methods. Since the equilibrium shape of liquid surfaces is determined by balance if surface tension and gravitational forces, analysis of drop or bubble shape may be used to determine surface

tension. The rise of liquid in capillary or the pull on a thin vertical plate partially immersed in the liquid may be determined and used to calculate the surface tension quite accurately. Less accurate values of surface tension may be obtained from measurements of moving liquid surface. These methods include studies of liquid jets, ripples, drop weight, and the force required to rupture a surface. [7]

The forces interacting with each molecule determine the final surface tension of a system. The stronger these forces, the higher the value of the surface tension. Thus, these inter molecular forces play a very important role in the value of the surface tension in a specific material. The intermolecular forces are generally divided to two main segments: [4]

1. Dispersive Forces, D;

    a. London Dispersive Forces

2. Polar Forces, P;

    a. Dipoles Forces

    b. Hydrogen Bonding

    c. Ionic Bonds

This showed that substances that have different surface tension, γ, are due to different contributions of D and P forces. Such as;

$$\gamma \text{ total } = \gamma D + \gamma P \tag{1.5}$$

1.1.3 Inter Molecular Forces

1.1.3.1 London Dispersive Forces

London Dispersive forces caused by movement of charges in non-polar molecules induction of electromagnetic attractive forces in the electron clouds of covalent molecules by distortion of charged cloud. Distortion is a result from the electric field produced by charge distribution in nearby molecule, Figure 1.5.

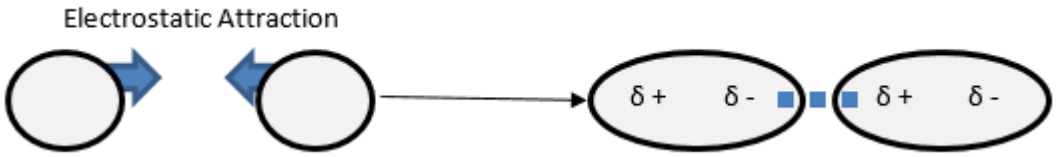

Figure 1. 5 Illustration of London Dispersive Forces of molecules

Size and shape of the molecules determine the magnitude of the London Dispersive Forces, the bigger the sizes, the higher the London Dispersive Forces. For examples, CH4,Methane is in gas form in room temperature but CH3-(CH2)4-CH3, Hexane, is liquid in room temperature and CH3-(CH2)8-CH3,octadecane, is in solid form in room temperature. It is shown in Figure 1.6 that, as for the influence of shape, it will also influence the value of the London Dispersive Forces value.

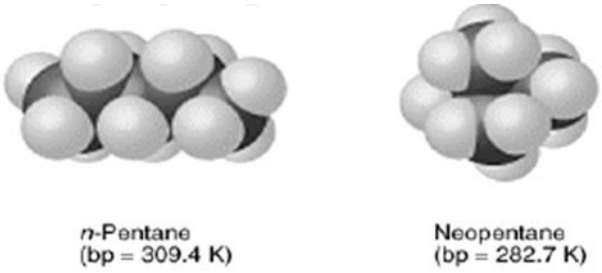

Figure 1. 6 Influence of shape on molecules London Dispersive Forces, Liner structural n-Pentane have larger dispersive forces because of its larger surface. Compact spherical structural neopentane have lower dispersive forces due to its shape and surface area. [4]

1.1.3.2 Dipoles Forces

Polar covalent molecules sometimes described as "dipoles", meaning that the molecule has two "poles". One end (pole) of the molecule has a partial positive charge while the other end has a partial negative charge. Dipole forces are caused by differences in electronegativity of an atom, where it has the ability to attract electrons. This action results in unequal sharing of electrons with creation of polar covalent bonding but the net charge remains the same.

Even though the total charge on a molecule is zero, the nature of chemical bonds is such that the positive and negative charges do not completely overlap in most

molecules. Such molecules said to be polar because they possess a permanent dipole moment.

The dipole moment, μ, is defined as the product of the total amount of positive or negative charge and the distance between their centroids. The centroids of the positive and negative charges in a molecule are determined in a manner similar to that used to determine the center of mass of a system.

As shown as Figure 1.7, The polar covalent bond that have the ability to perform the dipole forces are O-H, NH,C-Cl, C-F, C-O, C-N etc. The non- or low polar bonding will not have the ability to create this action and they are C-C, H-H, N-N, O-O etc. The overall dipole value depends on the molecule geometry.

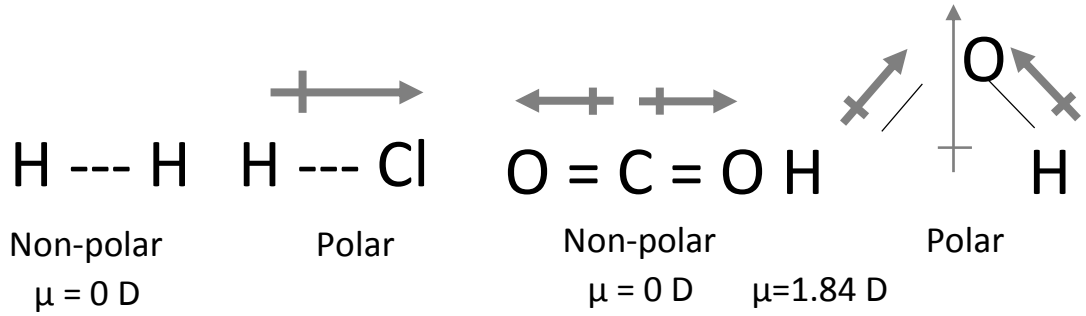

Figure 1. 7 Effects of symmetry and shape of molecules on Dipole Moment

Both phenomena on dispersive forces seem similar However, there are differences; London Dispersive Forces describes the phenomena that happened between different molecules/atom, even a symmetry molecule will have dispersive force. However, Dipole Moment describes the phenomena that created by an in-symmetry molecules (within the molecule) and later influencing other molecules.

1.1.3.3 Hydrogen Bonding

Hydrogen bond has a very strong dipole-dipole interaction (3-10 kcal/mol), typically happen in F-H, O-H and N-H bonds (H-donor). H-atom has strong affinity for non-bonding electrons (lone-pair electron) of other O- and N-atoms (H-acceptor).The hydrogen bond has only 5% or so of the strength of a covalent bond, however, when many hydrogen bonds form between two molecules (or parts of the same molecule), it

can be sufficiently strong as it can be quite stable. In Figure 1. 8, hydrogen bonds between water molecules are shown.

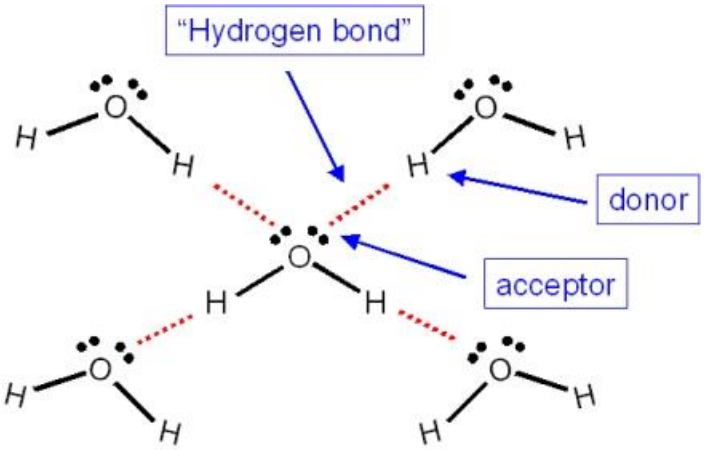

Figure 1. 8 Hydrogen bonds in water

1.1.3.4 Ionic Bonding

Ionic bonding is a type of electrostatic interaction between atoms which have a large electronegativity difference. There is no precise value that distinguishes ionic from covalent bonding, but a difference of electronegativity of over 1.7 is likely to be ionic, and a difference of less than 1.7 is likely to be covalent. Ionic bonding leads to separate positive and negative ions. Ionic charges are commonly between −3e to +3e. [9]

Ionic bonding best described using a simple electrostatic model. The electrostatic model is an application of the charge principles that opposite charges attract and similar charges repel. An ionic compound results from the interaction of a positive and negative ion, such as sodium and chloride in common salt.

In coatings, the most commonly known ionic bonding materials will be inorganic pigments where a Metal element carrying a positive charge and Oxygen carrying the negative charge form a strong bond with each other. However, in organic chemistry, the elements that bind together usually involved covalent bond. Ionic bonds can also be found in common salt where neutralization takes place. Ionic bonding is the strongest among all polar forces.

1.1.4 Capillary Action

As known that surface tension arises because of the intermolecular forces of attraction that molecules in a liquid exert on one another. These forces, which are between like molecules, are called cohesive forces. A liquid, however, is often in contact with a solid surface, such as glass. Then additional forces of attraction come into play. They occur between molecules of the liquid and molecules of the solid surface and, being between unlike molecules, are called adhesive forces. [8]

When the attractive forces are between unlike molecules, they are said to be adhesive forces. The adhesive forces between water molecules and the walls of a glass tube are stronger than the cohesive forces lead to an upward turning meniscus at the walls of the vessel and contribute to capillary action, in Figure 1.9.

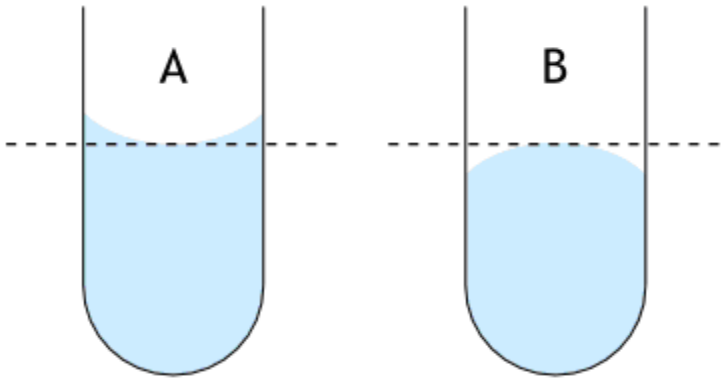

Figure 1. 9 A- Surface has a concave shape because liquid wets the surface and creeps up the side (like water), B- Liquid has a convex shape because of cohesive forces in liquid tend to draw it into a drop.(like mercury)

1.1.5 Interfacial Surface Tension

The understanding of interfacial surface tension is also important in paint and coating technology. In generally terms, interfacial surface tension is defined as surface tension at the surface separating two non-miscible materials.

Interfacial or surface tension exists when two phases are present. These phases can be solid-liquid, γSL; liquid-vapor, γLG; or solid-vapor, γSV. Interfacial tension is the force that holds the surface of a particular phase together and is normally such as surface tension.

Fowken equations shown below can be used to measure and calculate interfacial surface tensions. This equation will be explained under contact angles in next section.

$$\gamma SL = \gamma S + \gamma L - 2\left(\gamma S_D \times \gamma L_D + \gamma S_P \times \gamma L_P\right) \quad (1.6)$$

1.2 SUPERHYDROPHOBICITY

1.2.1 Introduction to Superhydrophobicity and Its History

Superhydrophobicity is an effect where surface roughness and chemical composition combine to generate unusual water repellent surface, causing water to bounce and roll off the surface. [10] Numerous studies have confirmed that this combination of micrometer-scales and nanometer-scale roughness, along with a low surface energy material leads to apparent Water Contact Angles (WCAs)>150°, a low sliding angle and the self-cleaning effect. [11] Surfaces that have these properties are called "superhydrophobic."

Superhydrophobic self-cleaning was first observed on the leaves of the (Indian) Lotus, Nelumbo nucifera. Which show small wax crystals on the top of waxy bumps. [12] Biological tiny structures have been observed on many kinds of surfaces such as lotus leaves, rice leaves, butterfly wings, mosquito eyes, moth eyes, cicada wings, red rose petals, gecko feet, desert beetle, spider silks, and fish scales which exhibit excellent hydrophobicity and/or superhydrophobicity. [11] According to the study of Neinhous and Barthlott, there are more than 200 plant species of which the surfaces exhibited water repellent property. [13] Such natural structures offer new insights into the design of artificial superhydrophobic structures. These are highly efficient at self-cleaning and repel a range of water-based liquids. Unlike natural structures, they are not sensitive to condensation and physical damage. This is a major advantage over artificial surfaces that wear away and become less effective over time. Both the chemistry of the surface and the shape must be maintained to preserve a superhydrophobic effect and waxes are good at both, being able to reorder when warm and dry to hide hydrophilic groups and regenerate surface structure.[12]

These surfaces are of special interest, because properties such as anti-sticking, anti-contamination, and self-cleaning are expected. These proper- ties are attractive for

many industrial and biological applications such as anti-biofouling paints for boats, antis-ticking of snow for antennas and windows, self-cleaning windshields for automobiles, microfluidics, lab-on-a-chip devices, metal refining, stain resistant textiles, anti-soil- ing architectural coatings, dust-free coatings on building glasses and so on. [10]

Since the early 1940s researchers have been interested in the wetting properties of surfaces, with more and more focus on the applications of such knowledge being brought about by technology and industrial applications of the 1990s. The number of methods reported in the literature to produce materials/ surfaces/ coatings presenting superhydrophobic properties has increased substantially over the past decade. [12] Many of the preparation techniques are simple, inexpensive; however, some of them involved multistep procedures and harsh conditions, or required specialized reagents and equipment. [10] The various methods for the preparation of biomimetic superhydrophobic surfaces since last two decades have been reported by Latthe S and collaborators. Some of the known process are phase separation, electrochemical deposition, template method, Emulsion, plasma method, crystallization control, chemical vapor deposition, wet chemical reaction, sol-gel processing, lithography, electrospinning, solution immersion and so on. [10]

1.2.2 Theoretical Background

1.2.2.1 Contact Angles

When a liquid rests on a surface, some angles are formed between the solid/liquid, liquid/air and solid/air. The wettability of a flat surface is founded by these contact angles (CAs). The angle between liquid/solid interfacial surface and liquid/air interfacial surface is expressed as Water Contact Angle (WCA), θ, which is defined by Young's Equation;

$$\gamma LA \; x \; cos\theta = \gamma SA - \gamma SL \tag{1.6}$$

where γLA, γSA and γSL refer to the interfacial surface tensions and A as liquid, solid and air, respectively. This equation can be applied only to a flat surface. The WCA on a perfectly smooth and chemically homogenous solid surface is given by Young's equation. [10]

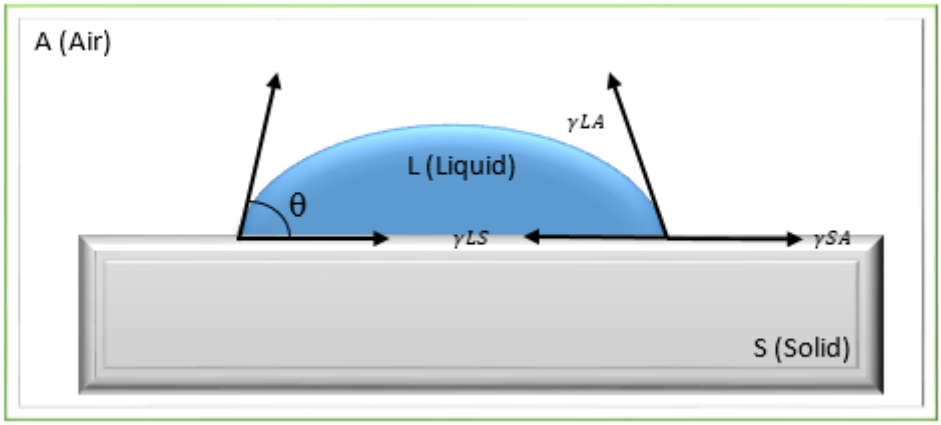

Figure 1. 10 Cross-section of a drop on a flat surface with the contact angle θ. Contact angles also form at the edge of larger pools of water, in tubes, at bubbles on underwater surface and any other configuration where a liquid interface meets a solid.

The equilibrium angle that forms is known as Young's angle after a theory proposed by Young, but not actually formulated in his work. [12] Young's equation can be considered as a force balance of lateral force on a contact line. Due to this, Young's angle can be defined as result of thermodynamic equilibrium of the free energy at the three phases interphase.

In a perfect system the contact line cannot sustain any lateral force, so will always move to a position where the forces balance. This is achieved mathematically by taking a components of the surface, at right angles to the contact line, as shown in Figure 1.10.

Depending on the value of CA, surface are called as; hydrophilic (CA < 90°), hydrophobic (CA ≥ 90º) or superhydrophobic (CA ≥ 150º). For small drops on a flat surface the drops form spherical caps, spheres intersection the surface. External factors such as electric fields, may also influence the drop shape, with gravity playing a role in distorting larger drops. At the contact angle tends to the Young angle except when the contact line is moving relatively rapidly. In most systems there is a certain uncertainty in contact angle known as contact angle hysteresis. [12]

1.2.3 Contact Angle Hysteresis

In practice, two types of CA values are used: static and dynamic CAs. For a flat surface, static contact angle is close to young's angle. Dynamic contact angles are non-

equilibrium CAs. Static CAs are obtained sessile drop measurement, where a drop deposited on the surface and the value obtained by a goniometer. [14] Dynamic CAs are measured during the advancing (growth, θa) and receding (shrinkage, θr) of water droplets. Differences of these angles is defined as contact angles hysteresis (Δθ).

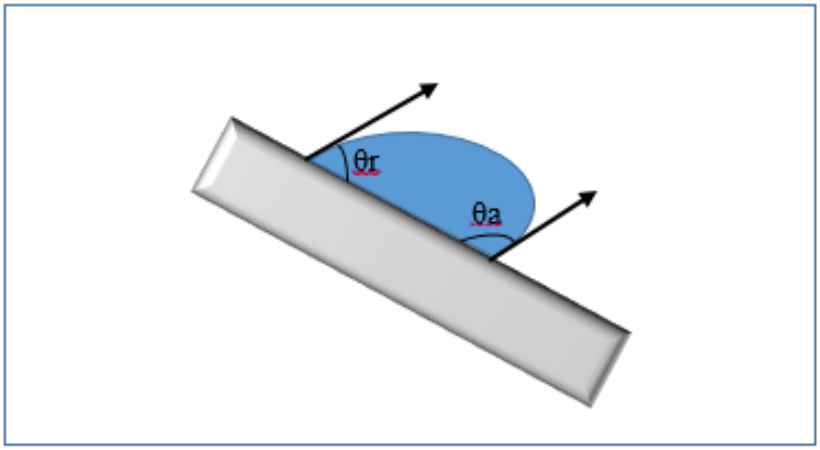

Figure 1. 11 Advancing or Growth angle at the front and Receding or Shrinkage angle

When a drop on an escarpment surface slide slowly, advancing and receding angles are formed, as shown as Figure 1.11. In practice, due to chemical heterogeneity, roughness, geometrical factors and speed of movement, many surfaces show much larger hysteresis. [12, 14]

1.2.4 The Effect of Roughness

The behavior of a water droplet on a rough surface is explained at previous section. Wetting of realistic surfaces which are rough and chemically heterogeneous is more complex. [10] Water can penetrate the asperities (or suspend above the asperities). In this case, much higher CA are observed than CA obtained at flat surfaces. The basic guidelines on the effect of surface roughness for CA was done by Wenzel and Cassie & Baxter. These two situations are named the Wenzel state (penetration) and Cassie-Baxter state (suspension).

1.2.4.1 *Fully Wet Surface; Wanzel's Equation*

Wenzel developed a model where the liquid may completely penetrate into rough grooves, as shown in Figure 1.12. At thermodynamics equilibrium, there is a linear relationship between the apparent CA of the surface and the roughness factor of given surface. The increasing surface area of the interface means that the advancing contact angle of greater than 90º increases, whereas that of one below 90º decreases. A surface with exactly 90º CA would show no effect of roughness. This type of wetting can, therefore, be considered to be an amplification of the properties of the surface by the roughness. [12] The CA of a rough surface of this type is calculated by Wenzel's equations;

$$cos\theta w = r\ x\ cos\theta = r\ x\ (\frac{\gamma SA - \gamma SL}{\gamma LA}) \tag{1.7}$$

where θw corresponds to the apparent contact angle, θ is the Young's CA on a similar smooth surface and r represents the roughness factor, defined as the ratio between the actual and projected surface area. For a perfectly smooth surface r = 1, and for a rough one r > 1. Fallowing Wenzel's prediction, for a hydrophobic surface θw > θ > 90º and for a hydrophilic surface θw < θ < 90º. Roughness enhances both hydrophobicity and hydrophilicity depending on the nature of corresponding flat surface. [14]

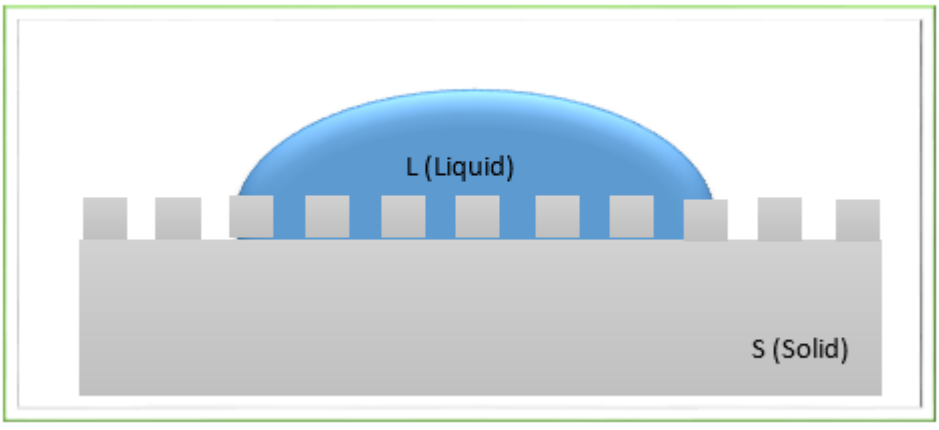

Figure 1. 12 Wenzel state, liquid penetrates into the spikes

However, when θ > 90º, under some roughness condition, air bubbles may be trapped in the rough grooves. In this case, the liquid droplet is actually situated on a composite surface, and the wetting behavior is described by Cassie & Baxter.

1.2.4.2 Bridging the Roughness; Cassie – Baxter's Equations

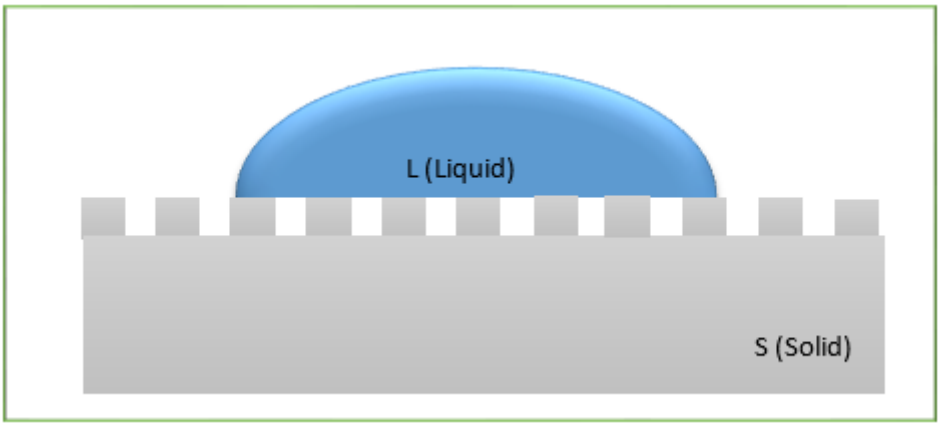

Figure 1. 13 Cassie – Baxter state, liquid drop suspends on the spikes

The Cassie- Baxter state also known as a composite or heterogeneous state, is wetting state, where it is considered that grooves under droplet are filled with vapor instead of liquid, as shown in Figure 1.13. If the surface is roughened it eventually becomes energetically favorable for the liquid to sit on the top of the roughness and reduce the area of the interface.

The first description for CA on a surface of this type was formulated in 1944 by Cassie & Baxter. In this case, the liquid-surface interface is actually an interface consisting of two phases such as liquid - vapor (in figure 1.13) or liquid – solid.

As a result of the suspension of the water droplet on the asperities, in the Cassie-Baxter model, the apparent CA is the sum of all the contributions of the different phases as described by fallowing equations;

$$cos\theta c = f1\, cos\theta 1 + f2\, cos\theta 2 \tag{1.8}$$

where, θc is the apparent CA, f1 and f2 are the surface fraction of the phase 1 and phase 2, respectively; θ1 and θ2 are the CA on phase 1 and phase 2, respectively. This equation is the general form, which also applies when there is no roughness. For a rough surface containing only one type of asperities, given f is the solid fraction, defined as the fraction of the solid surface that is wetted by liquid. Then the air fraction is (1- f). With θ=180º for air, the resulting CA can be calculated by fallowing equation:

$$\begin{aligned} cos\theta c &= f cos\theta + (1-f) cos180° \\ &= f cos\theta + f - 1 \end{aligned} \tag{1.9}$$

The parameter f ranges from 0 to 1, where at f=0 the liquid droplet does not touch the surface at all and f=1 the surface is completely wetted, the same as the behavior of a flat surface. When a droplet is in the Cassie-Baxter, the small contact area between the liquid droplet and solid surface allows the droplet to roll easily over the surface. [10]

1.2.5 Functional Properties of Superhydrophobic Surfaces

Over the past years attention has moved towards developing advanced materials with properties suitable for a range of applications; either for research or industrial requirements. A number of commercial products making use of superhydrophobicity is already available on the market, with others currently under development. In addition, many patents have been granted for various possible applications of self-cleaning surfaces. Many of these products are used primarily for their superhydrophobic self-cleaning abilities, such as materials used in construction for windows or roofing tiles. Materials coating used in this industry are also widely available, with paints used to form a barrier against bio-fouling or graffiti-resistant layers. The use of non-wettable textiles is also progressing rapidly.

Superhydrophobic films have wide spectrum of applications, and are used not only for resisting water, but also most areas such as list below.

- Prevent contamination
- Evaporation and condensation resistance
- Fog resistance
- Anti-fouling

- Anti-corrosion
- Transparent and anti-reflective properties
- Anti-icing (frost and ice resistance)

Their applications have extended to some fields, such as biocompatibility, lubricity and durability of materials, for their low free energy surface. [15]

1.2.5.1 Anti-icing

Ice and wet-snow adhesion to outdoor surfaces is known to cause several serious problem for most of application area such as power transmission line. Even though there is no material to completely prevent ice or snow accretion on its surface, some coating are believed to provide reduced adhesion. [16]

Frost formation occurs via two main process: nucleation and crystal growth, being dependent upon the water vapor overcoming a Gibbs free-energy barrier. Freezing of water has been shown to be significantly delayed when depositing droplets onto cooled superhydrophobic surface. Microtextures were found to delay freezing with drops rolling off without leaving behind a film of ice or freezing. [12]

The low contact area and air gap is thought to reduce the transfer of heat from the liquid to the surface, preventing freezing. [12]

According to several recent studies, [11, 12, 13, 16, 15, 17] anti-icing properties is needed a surface which repels water more effectively than any flat surface. The water repellency is based on surface roughness caused by different microstructures, together with the hydrophobic property of wax crystals. [13] This is possible if the surface of a hydrophobic solid is roughened; the liquid/solid interfacial area is increased and the low surface energy. This properties and mechanisms will be explained extensively in the fallowing parts.

1.2.6 Production Methods of Superhydrophobic Surfaces

To fabricate the superhydrophobic surfaces, recently many elegant chemical and physical routes have been developed. Many routes to prepare superhydrophobic surface

require complicated, sometimes costly equipment, although some surfaces can be fabricated quite easily. [10]

There are two basic mechanism to increase the contact angle; one of them is to change the surface chemistry that can lower the surface energy sufficiently, which generally referred to as the chemical method. The other one is to increase the surface roughness so as to increase the true or effective surface are resulting in an increase in nominal surface energy, which is known as the geometrical method. For the formation of superhydrophobic films or coatings, modification of surface chemistry is always combined with surface roughness enhancement [15]

To make superhydrophobic surfaces can be simply divided into two categories;

• Modifying a rough surface with a material of low surface energy

• Making a rough surface from a low surface energy material

1.3 CONTACT ANGLE MEASUREMENTS

Over the years a large number of techniques have been developed to probe different aspects of the physics and chemistry of surfaces, however, only a few have found wide application in basic surface science and applied surface analysis. The choice of the technique depends upon the type of the characterization to be made. Among the most widely used methods are X-ray photoelectron spectroscopy (XPS) and Fourier transform infra-red spectroscopy (FTIR) are used to study the surface chemical composition. Similarly, scanning electron microscopy (SEM) and atomic force microscopy (AFM) are used to investigate the surface morphology of the material in atomic scale. These methods require relatively expensive equipment, skilled technicians and sophisticated techniques to interpret data. Measurement of surface energy of the solid can also provide a good understanding of the surface properties of a solid using relatively a very simple approach. The surface energy of a solid can be determined from the measurement of contact angle of a pure liquid drop on that solid. Contact angle measurement has been used in the study of surface energy, wettability and adhesion of low surface energy materials. [18]

Wettability studies usually involve the measurement of contact angles as the primary data, which indicates the degree of wetting when a solid and liquid interact. Small

contact angles (<< 90°) correspond to high wettability, while large contact angles (>> 90°) correspond to low wettability, [19] as shown in Figure 1.19;

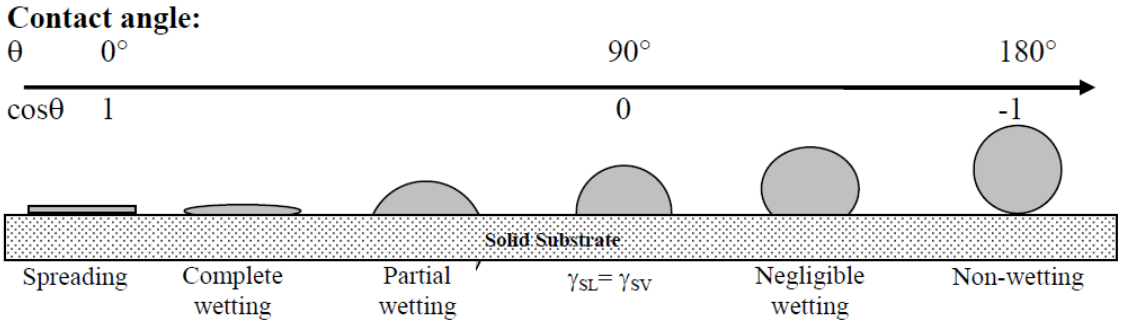

Figure 1. 14 Liquid drops on solid surface [20]

According to the fundamentals science behind wetting and contact angle phenomena, there are various techniques used to measure contact angle. Most of these techniques can be classified into two main groups; the direct optical method and indirect force method.

Wettability of solid-fluid-fluid interfacial phenomena is often characterized by measuring the contact angle formed between a liquid drop and a solid surface. This measurement is considered to be a relatively simple, useful, and sensitive tool for assessing hydrophobicity or hydrophilicity of a surface, surface heterogeneity, surface roughness, solid surface energy, liquid surface tension, and line tension. [20]

One of the most popular methods for measuring the contact angle is the sessile drop method, which involves depositing a liquid drop on a smooth solid surface and measuring the angle between the solid surface and the tangent to the drop profile at the drop edge.

1.3.1 Direct Contact Angle Measurement by Optical Method – Contact Angle Goniometer

Bigelow et al. [21] set up a simple and convenient instrument, which they referred to as a "telescope-goniometer" to measure contact angles of various liquids on polished surfaces. Later, the first commercial contact angle goniometer, designed by Dr. William.A. Zisman of the United States Naval Research Laboratory in Washington,D.C., was manufactured by ramé-hart instrument company in the early 1960s (Figure. 1.15).

The original manual contact angle goniometer used an eyepiece with microscope. The current generation of contact angle instruments uses cameras and software to capture and analyze the drop shape and are better suited for dynamic and advanced studies. [22]

Figure 1. 15 A rame-hart contact angle telescope-goniometer [19]

The use of the term "contact angle goniometer" in connection with photographic or video capture systems focused on sessile drops is often a misuse of the word goniometer, as most systems do not measure angles. Images are captured and operator imposed asymptotes are drawn, and the software connected with the drawing actions then computes the angle between these operator imposed lines, the contact angle. [22]

Figure 1. 16 Optic Goniometer (or contact angle meter) used by author.

In Figure 1.16, one of the modern optic Contact angle meter, goniometer, is shown. Side-looking measurement of contact angle by sessile drop method is done by this equipment. Working principles is shown in Figure 1.17.

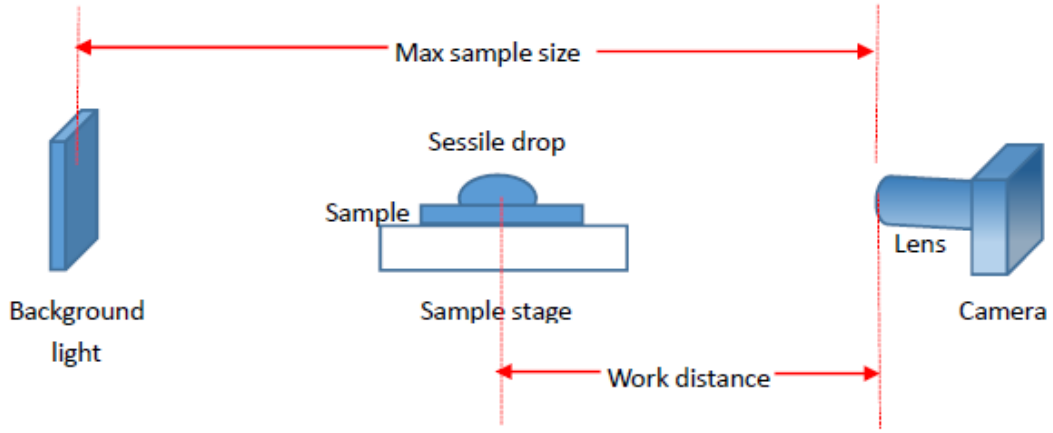

Figure 1. 17 Working principles of sessile drop method by goniometer

The equipment consists of a horizontal stage to mount a solid or liquid sample, a micrometer pipette to form a liquid drop, an illumination source, and a telescope equipped with a protractor eyepiece. The measurement was achieved by simply aligning the tangent of the sessile drop profile at the contact point with the surface and reading the protractor through the eyepiece. Over the years, modifications of the equipment have been made to improve the accuracy and precision. A camera can be integrated to take photographs of the drop profile so as to measure the contact angle at leisure. The use of relatively high magnifications enables a detailed examination of the intersection profile. A motor-driven syringe can be used to control the rate of liquid addition and removal to study advancing, receding, or dynamic contact angles. [19]

This direct optical method is advantageous because of its simplicity and the fact that only small amounts of liquid (a few microliters) and small surface substrates (a few square millimeters) are required. On the other hand, there is a relatively higher risk/impact of impurities due to the small size of the liquid and substrate. As for accuracy and reproducibility, the measurement relies on the consistency of the operator in the assignment of the tangent line, which can lead to significant error and inconsistency between multiple users. It is suggested that the telescope be tilted down slightly (1 to 2°)

off the horizon so that the near edge of the sample stage (out of focus) is out of the line of sight, and a portion of the profile reflected by the substrate surface is brought into focus, which prevents forming a fuzzy liquid-substrate contact line in the profile. A background light is always used to assist observation, while a specific light source is selected to avoid undesired heating of the liquid or substrate.

To establish an advancing contact angle, it is best to slowly grow the sessile drop to a diameter of approximately 5 mm using a micrometer syringe with a narrow gauge stainless steel or Teflon needle. The needle must remain in the liquid drop during measurement to avoid undesired vibration. The needle diameter should be as small as possible so it does not distort the drop profile shape. Because, the drop might be unsymmetrical, it is advisable that contact angles be measured on both sides of the liquid drop profile, and to use the averaged result. For a relatively large substrate, contact angles should be measured at multiple points to give an average value that is representative of the entire surface.

The direct goniometer method suffers from another serious limitation because small contact angles (below 20°) cannot be accurately measured due to the uncertainty of assigning a tangent line when the droplet profile is almost flat. Also, the imaging device only focuses on the largest meridian section of the sessile drop, which means the profile image reflects only the contact angle at the point in which the meridian plane intersects the three-phase line. In addition, the dependence of the contact angle on the drop size causes a systematic problem. Despite all of these issues, the goniometer method is considered to be the most convenient method if high accuracy is not required. It is generally recognized that the direct measurement of sessile drop contact angles with a telescope-goniometer can yield an accuracy of approximately ±2°. [19] In Figure 1.18, there are some results of contact angles measurement on different surfaces. [23]

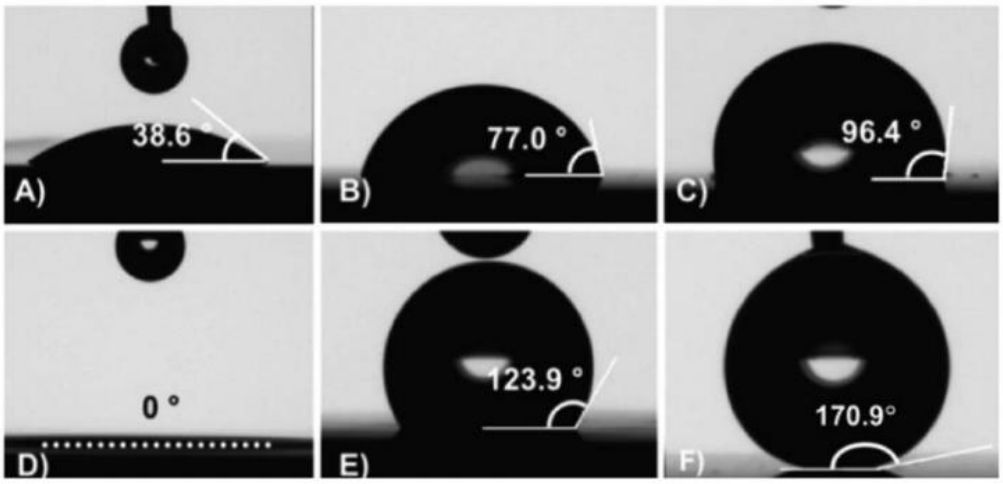

Figure 1. 18 Pictures and contact angle measurements of a 6 ml water drop on: (A) a smooth oxidized silicon wafer; (B) a smooth bare silicon wafer; (C) a smooth PFOS-coated silicon wafer; (D) an oxidized SiNW_5+15 surface (the drop spreads out with a contact angle of approximately 0, dotted line); (E) a bare SiNW_5+15 surface; and (F) a PFOS-coated SiNW_5+15 surface. The ESI includes videos of drops falling on substrates (D) to (F). [6]

CHAPTER 2

EXPERIMENTAL PROCEDURE

2.1 MATERIALS

Some different polymer resins are used for nanocomposite matrix structure. One of them, Hardsil AM, was provided by Gelest Inc. and the others were provided by Dow Corning Chemicals.

All chemicals were chosen due to their characteristic properties such as viscosity, structure, hardness, curing temperature and time and adhesion ability. Contact angles of the polymers will be shown in next section.

Below is a list of polymers which are used in this work and their properties.

Polymers	*Composition*	*Viscosity*	*Curing*
Hardsil AM	Polysilsesquioxane T-resin	5-15 cst	30-60 min. / 125-140 ˚C
1965	Silicone elastomer	115 mPa.s	RT curing
2577	Silicone in solvent	950 mPa.s	RT curing
9189	Silicone Sealant	----	High humidity at RT
9187	Silicone Sealant	1150 mPa.s	RT curing
2620	Silicone resin solution	350 mPa.s	10 min / 60 ˚C
1953	Silicone elastomer	350 mPa.s	RT curing

Table 2. 1 The list of used polymer for matrix and some of the their properties

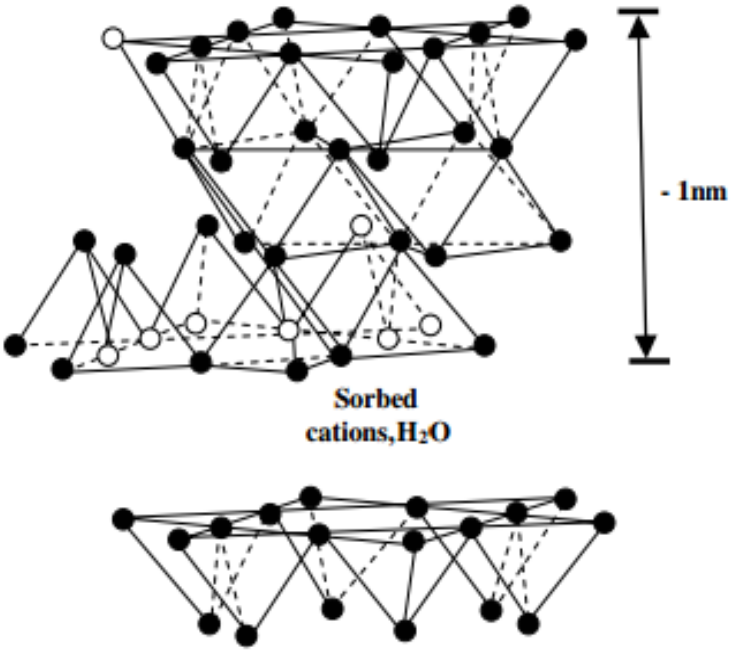

Figure 2. 1 Structure of MMT clay. [25]

Montmorillonites, are also referred to as Bentonites, are used as nano-sized reinforced particles in the nanocomposite structure. MMTs are very soft minerals that typically form in microscopic crystals and forming a clay. Montmorillonite, a member of the smectite group, is a 2:1 clay, meaning that it has two tetrahedral sheets sandwiching a central octahedral sheet. [24] The particles of MMTs are plate-shaped which has approximately one nanometer diameter, shown in Figure 2.1. Because of their layer by layer structure, particle size can be reduced under 100 nm and it has high ion exchange capacity which is easier to modification.

In addition to MMT, hydrophilic silica particles are used to understand the effects of the particle size on composite structure and properties. Hydrophilic silica particles were bought from Sigma – Aldrich with 682659 ALDRICH product code. Using of MMT clay is more logical due to their economic advantages and high ion exchange capacities. However, silica particles are also more effective due to their particle size distributions and uniformities. As it is known that, surface ratio is one of the most important parameters for reinforced materials in nanocomposite structure, especially in surface applications such as superhydrophobicity.

There are two different kinds of surfactants were used for two purposes; superhydrophobicity and corrosion resistivity. Owing to the fact that one of the most important parameters is surface energy for surfactants, two major surfactants were choosen; FDTS (Perfluorodecyltrichlorosilane), and OTMS (Octadecyltrimethoxysilane) As it is known that, surfactants which have CH3 and CF3 groups in their chemical structures, have smaller surface energy. As it shown in Figure 2.2, they have low surface energy due to their structures and can be used for superhydrophobicity applications.

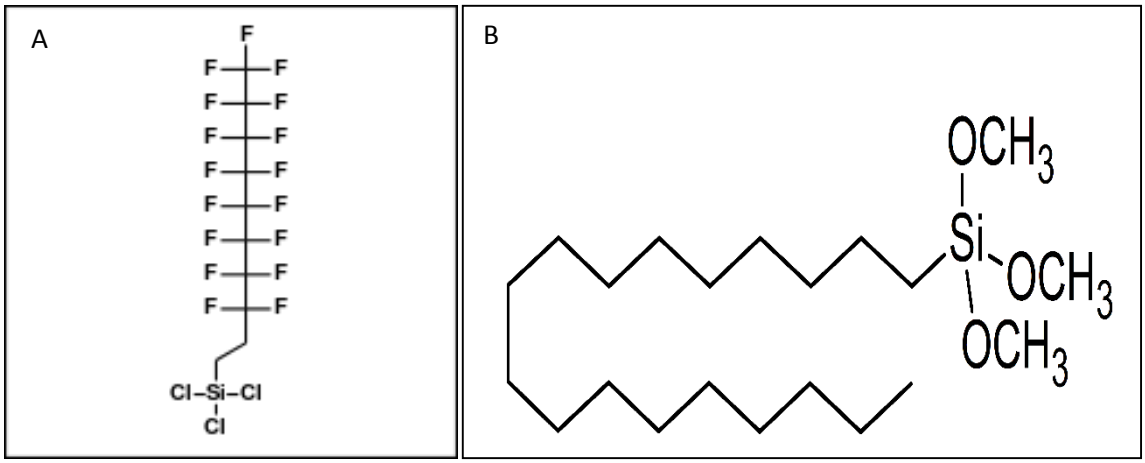

Figure 2. 2 Structure of Surfactants. A- FDTS, Perfluorodecyltrichlorosilane B- OTMS, Octadecyltrimethoxysilane

BTA and TTA are corrosion inhibitors. Their structure is also shown in Figure 2.3. FDTS and OTMS are dispersed in hexane and BTA and TTA are dispersed in IPA.

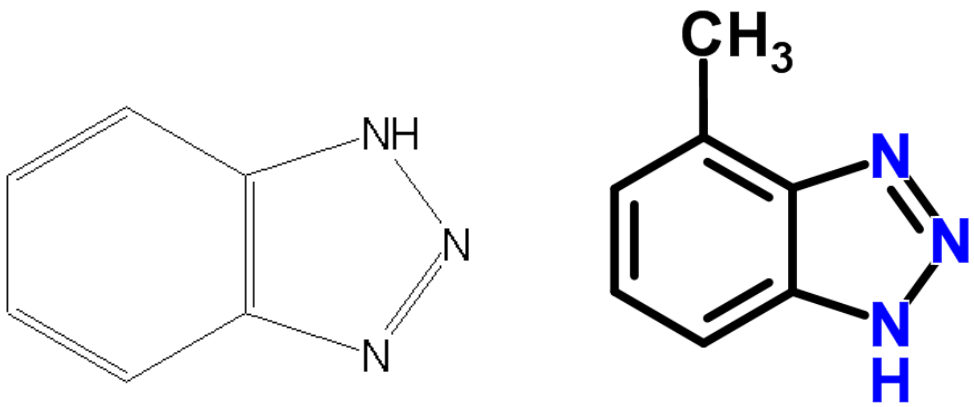

a) Benzotriazole b) Tolytriazole

Figure 2. 3 Structure of BTA (a) and TTA (b)

2.2 PREPARATION OF NANOPARTICLE/POLYMER NANOCOMPOSITES

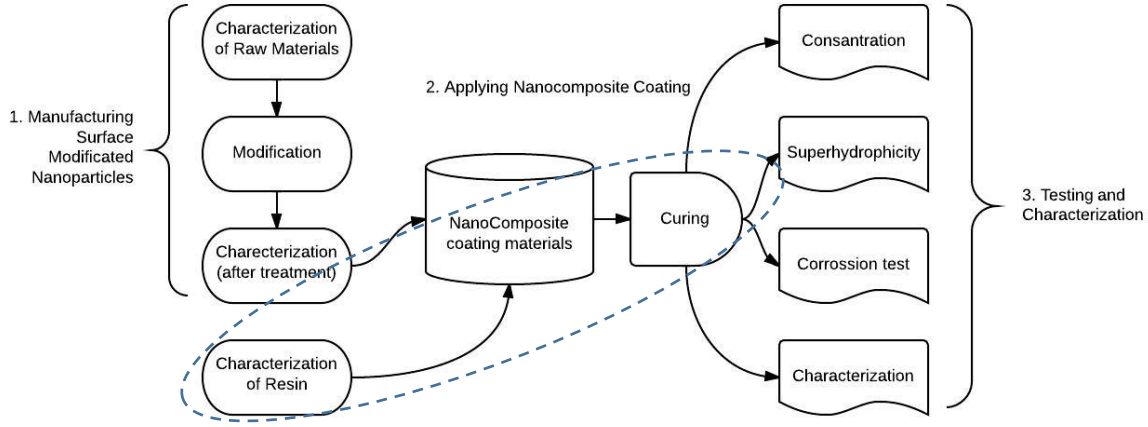

Figure 2. 4 Flowchart of Experimental Procedure

When size of particles reduced to nano-scale, the properties of materials change directly because of their volume/mass ratio at the surface. In this work, modified nanoparticles doped to the polymer as reinforced materials for anti-corrosion and anti-icing purposes. There are three major steps applied to produce superhydorphobic and anti-corrosive nanocomposite coating materials for high voltage transmission cables. As shown in flowchart of experiments, in Figure 2.4, these milestones are;

- Manufacturing Surface Modified Nanoparticles
- Applying Nanocomposite Coating
- Testing and Characterization

These three steps were applied sequentially and repeated several times to optimize the results and find the best values for parameters, such as concentration, curing time and temperature, coating method.

2.2.1 Manufacturing Surface Modified Nanoparticles

2.2.1.1 Size Distribution of Particles

Size distribution measurement is found by laser light scattering techniques in Malvern nanoZS equipment. Low concentrated samples were prepared in distilled water. As it is shown in Figure 2.5 and Figure 2.6 size distributions of MMT and silica particles

are respectively about 400-450nm and 165nm. Size distribution range of MMT is not narrow like silica particles and particle size ratio is about 2:1.

These particles improve the properties of materials both mechanically and surface treatment for superhydrophobicity or anti-corrosivity. As it is well known, both uniformity and particle size of reinforced materials are some of the most important parameters for particle based polymer nanocomposites. For the formation of superhydrophobic films or coatings, modification of surface chemistry is always combined with surface roughness enhancement so surface roughness is as important as surface energy.

In this type coatings, surface roughness is occurred by particles stayed on surface. According to results, using of silica particles can be more effective than MMT particles because of their particle size and distribution.

Z-Average (nm):	654,6246	Derived Count Rate (kcps):	1545,41765117...
Standard Deviation:	22,89105	Standard Deviation:	22,9213286121...
%Std Deviation:	3,49682	%Std Deviation:	1,48318020017...
Variance:	524	Variance:	525,387305345...

Size d.nm	Mean Number %	Std Dev Number %	Size d.nm	Mean Number %	Std Dev Number %	Size d.nm	Mean Number %	Std Dev Number %	Size d.nm	Mean Number %	Std Dev Number %
0,4000	0,0	0,0	5,615	0,0	0,0	78,82	0,0	0,0	1106	1,0	0,7
0,4632	0,0	0,0	6,503	0,0	0,0	91,28	0,0	0,0	1281	0,5	0,5
0,5365	0,0	0,0	7,531	0,0	0,0	105,7	0,0	0,0	1484	0,3	0,3
0,6213	0,0	0,0	8,721	0,0	0,0	122,4	0,0	0,0	1718	0,2	0,2
0,7195	0,0	0,0	10,10	0,0	0,0	141,8	0,0	0,0	1990	0,1	0,1
0,8332	0,0	0,0	11,70	0,0	0,0	164,2	0,0	0,0	2305	0,1	0,1
0,9649	0,0	0,0	13,54	0,0	0,0	190,1	0,3	0,4	2669	0,0	0,1
1,117	0,0	0,0	15,69	0,0	0,0	220,2	1,4	1,9	3091	0,0	0,0
1,294	0,0	0,0	18,17	0,0	0,0	255,0	3,9	3,8	3580	0,0	0,0
1,499	0,0	0,0	21,04	0,0	0,0	295,3	8,2	4,0	4145	0,1	0,0
1,736	0,0	0,0	24,36	0,0	0,0	342,0	13,3	1,1	4801	0,1	0,0
2,010	0,0	0,0	28,21	0,0	0,0	396,1	16,7	2,9	5560	0,1	0,0
2,328	0,0	0,0	32,67	0,0	0,0	458,7	17,1	4,6	6439	0,0	0,0
2,696	0,0	0,0	37,84	0,0	0,0	531,2	14,7	4,0	7456	0,0	0,0
3,122	0,0	0,0	43,82	0,0	0,0	615,1	10,5	2,1	8635	0,0	0,0
3,615	0,0	0,0	50,75	0,0	0,0	712,4	6,3	0,5	1,000e4	0,0	0,0
4,187	0,0	0,0	58,77	0,0	0,0	825,0	3,4	0,7			
4,849	0,0	0,0	68,06	0,0	0,0	955,4	1,8	0,9			

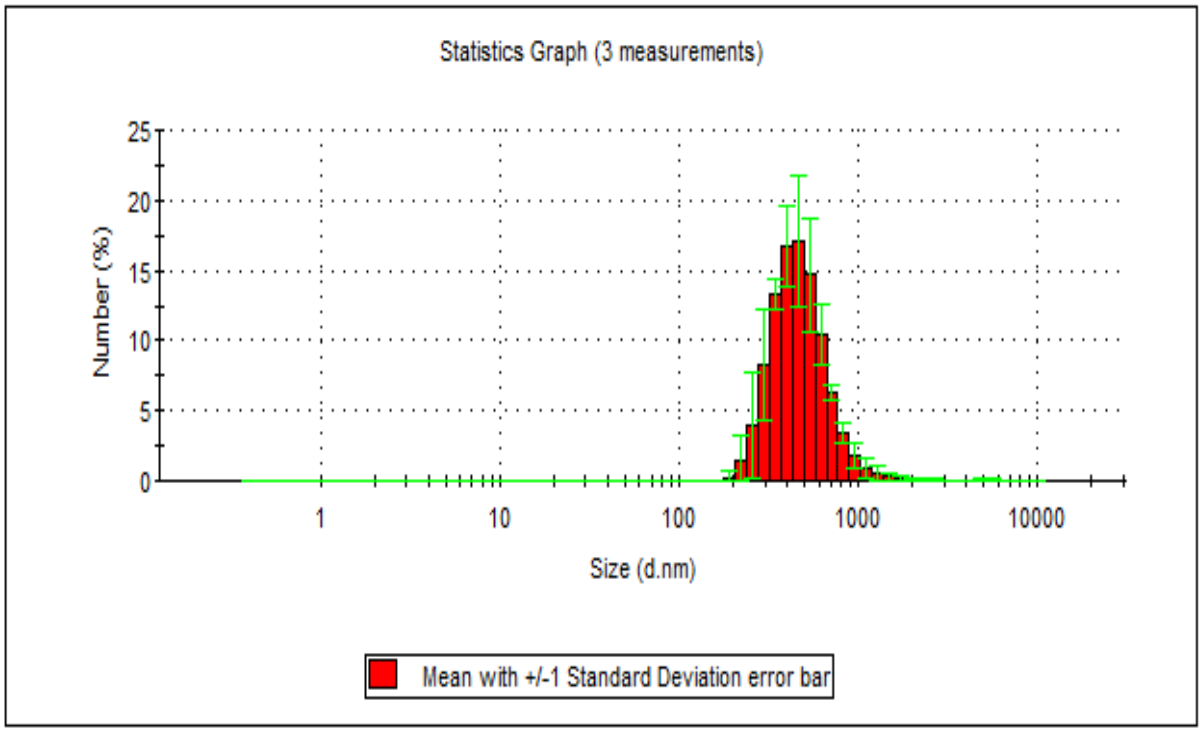

Figure 2. 5 Size Distribution of MMT Particles

Z-Average (nm):	380,1095	Derived Count Rate (kcps):	194,342676798...
Standard Deviation:	10,583	Standard Deviation:	1,13966148837...
%Std Deviation:	2,784199	%Std Deviation:	0,58641854025...
Variance:	112	Variance:	1,29882830808...

Size d.nm	Mean Number %	Std Dev Number %	Size d.nm	Mean Number %	Std Dev Number %	Size d.nm	Mean Number %	Std Dev Number %	Size d.nm	Mean Number %	Std Dev Number %
0,4000	0,0	0,0	5,615	0,0	0,0	78,82	0,0	0,0	1106	0,0	0,0
0,4632	0,0	0,0	6,503	0,0	0,0	91,28	0,0	0,0	1281	0,0	0,0
0,5365	0,0	0,0	7,531	0,0	0,0	105,7	0,0	0,0	1484	0,0	0,0
0,6213	0,0	0,0	8,721	0,0	0,0	122,4	5,9	5,7	1718	0,0	0,0
0,7195	0,0	0,0	10,10	0,0	0,0	141,8	19,7	13,9	1990	0,0	0,0
0,8332	0,0	0,0	11,70	0,0	0,0	164,2	27,8	9,0	2305	0,0	0,0
0,9649	0,0	0,0	13,54	0,0	0,0	190,1	23,1	5,2	2669	0,0	0,0
1,117	0,0	0,0	15,69	0,0	0,0	220,2	13,9	10,7	3091	0,0	0,0
1,294	0,0	0,0	18,17	0,0	0,0	255,0	6,6	8,5	3580	0,0	0,0
1,499	0,0	0,0	21,04	0,0	0,0	295,3	2,4	3,9	4145	0,0	0,0
1,736	0,0	0,0	24,36	0,0	0,0	342,0	0,5	0,9	4801	0,0	0,0
2,010	0,0	0,0	28,21	0,0	0,0	396,1	0,0	0,0	5560	0,0	0,0
2,328	0,0	0,0	32,67	0,0	0,0	458,7	0,0	0,0	6439	0,0	0,0
2,696	0,0	0,0	37,84	0,0	0,0	531,2	0,0	0,0	7456	0,0	0,0
3,122	0,0	0,0	43,82	0,0	0,0	615,1	0,0	0,0	8635	0,0	0,0
3,615	0,0	0,0	50,75	0,0	0,0	712,4	0,0	0,0	1,000e4	0,0	0,0
4,187	0,0	0,0	58,77	0,0	0,0	825,0	0,0	0,0			
4,849	0,0	0,0	68,06	0,0	0,0	955,4	0,0	0,0			

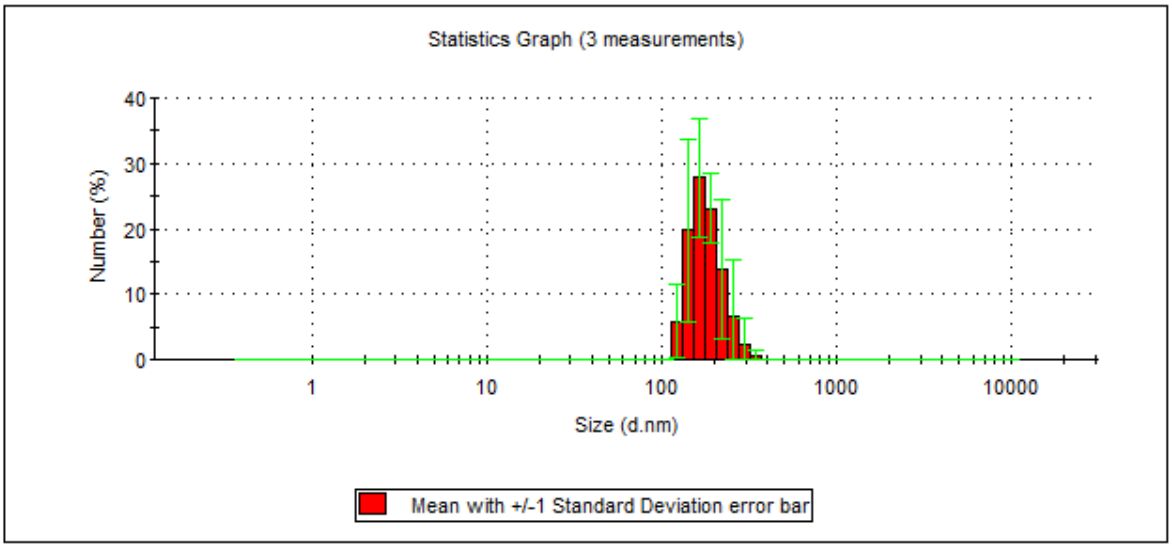

Figure 2. 6 Size Distribution of Silica Particles

2.2.1.2 Zeta Potential Titration

All measurements of zeta potential titration are also taken with same equipment, Malvern nanoZs, in zeta potential mode with zeta potential cuvette, Figure 2.7.

Solids in such emulsion or colloid systems have very high surface area. This type of titration is used for the zeta potential of these surfaces under different conditions. One of two important points is the iso-electric point that is the pH value at which the zeta potential is approximately zero. When the pH value is about the iso-electric point, colloids are usually unstable; the particles tend to coagulate or flocculate. The other one, the pH

value at which the zeta potential is maximum or minimum. That is the most stable point for colloids. Below of minimum value or above of maximum value, CMC (Critical Micelle Concentration) could be start.

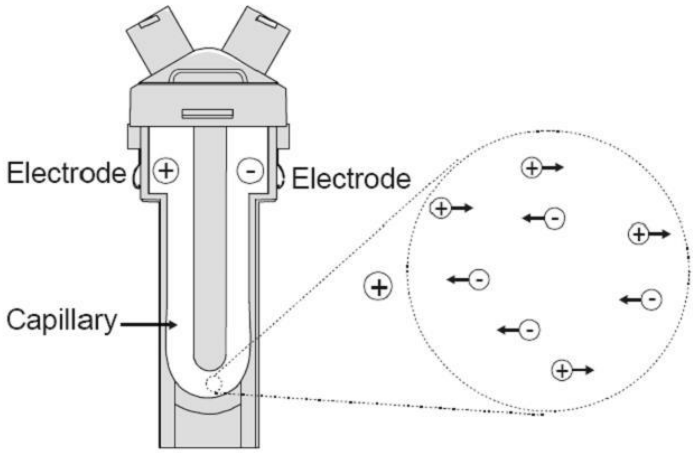

Figure 2. 7 Zeta Potential Measurement Cuvette and basically working Principles of System

Titrations for concentrated dispersions of MMT particles are shown in Figure 2.8. All measurements were repeated three times (M1, M2 and M3). It is seen that, there is no isoelectric points for MMTs because of their own surface charge. According to results of titrations graphs, MMT particles are more stable at approximately neutral pH, such as 6 – 7 pH. It is important that, the value of pH must stay such values for all modification processes, e.g. ion exchange, layer charge, getting more effective results about surface adsorption and preventing coagulate or flocculate. Unlike MMT, zeta potential titration of silica particles does not change importantly due to their structure and there is no important pH values.

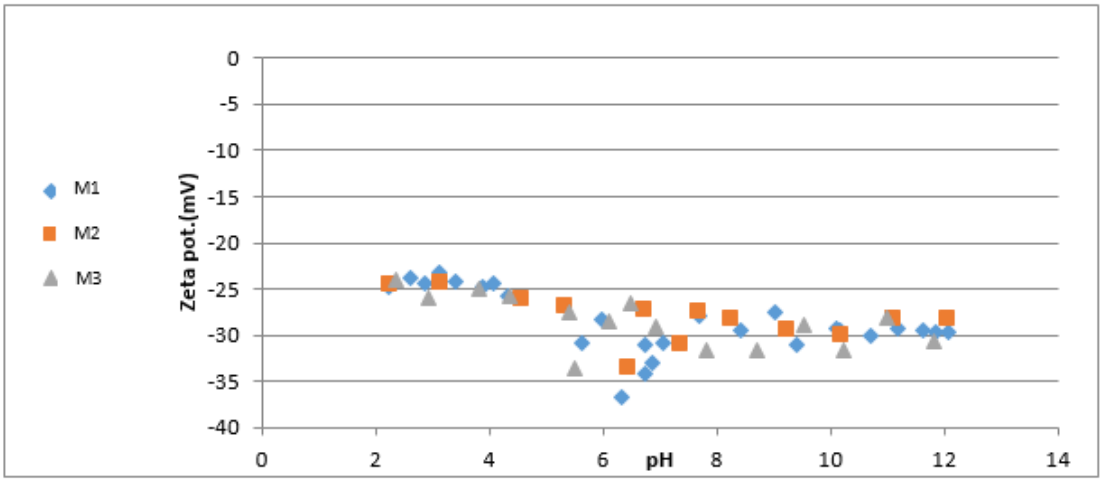

Figure 2. 8 Zeta Potential Titrations for concentrated dispersions of MMT particles

2.2.1.3 Surface Area Measurements – BET analysis

Surface area analysis of nano-sized clay particles was measured by gas absorption techniques at Erciyes University Technology Research Center. Results of MMT particles and silica particles are shown in respectively, Figure 2.9 and Figure 2.10. The results show that, silica particles have larger surface area than MMT particles because of their size.

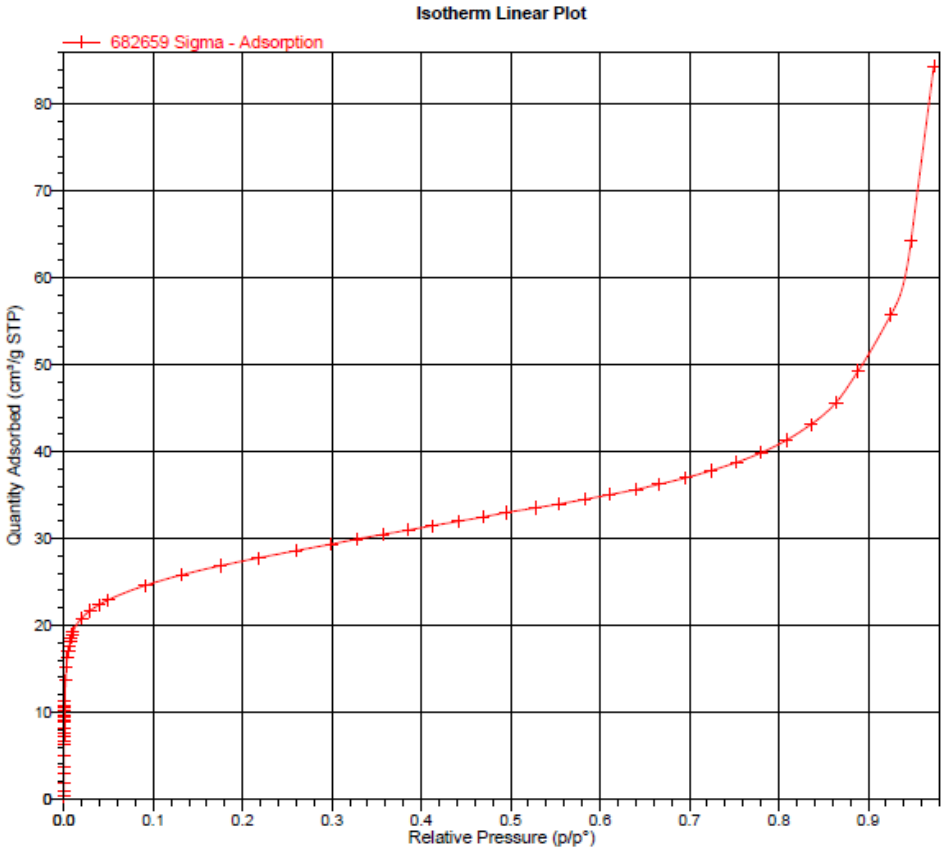

Figure 2. 9 BET analysis of MMT particles

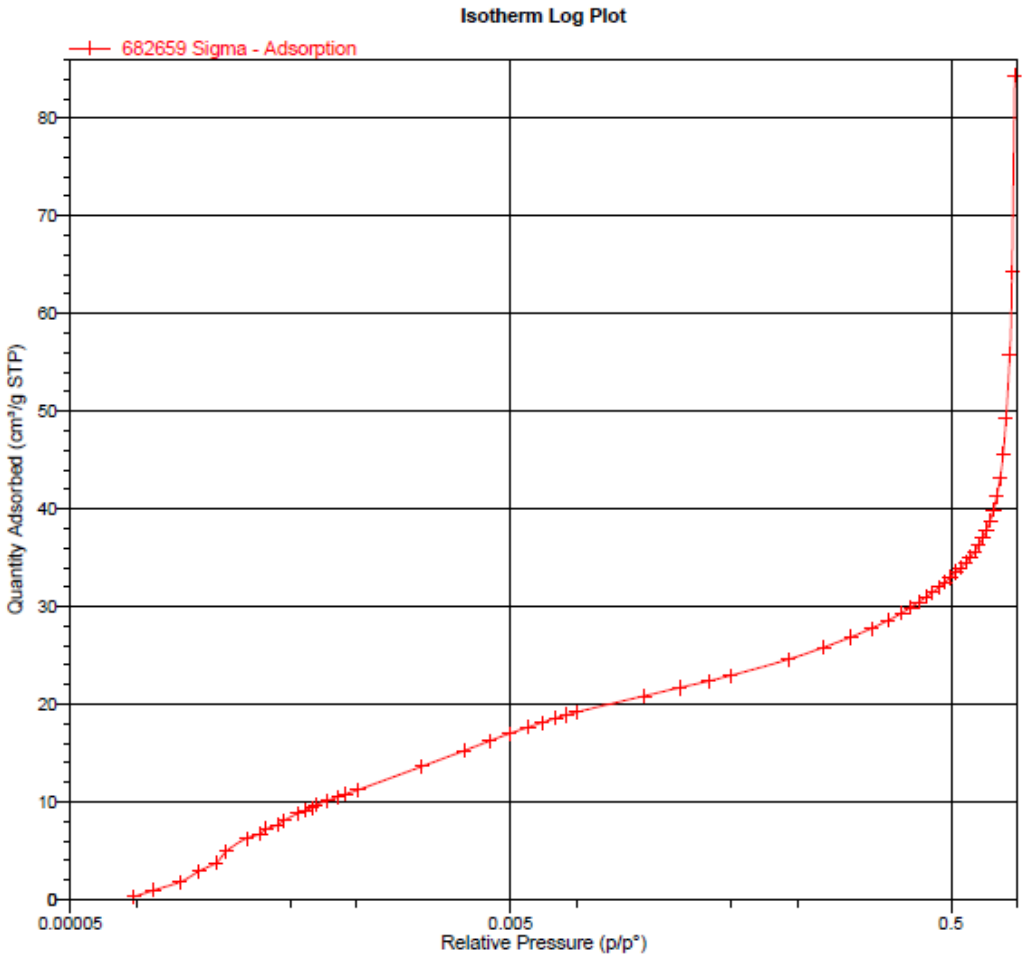

Figure 2. 10 BET analysis of Silica particles

2.2.1.4 Modification Process

The organophilic clays are not compatible with hydrophobic matrices as the d-spacing is extremely narrow and hence diffusion of polymer chains in the clay galleries is not possible. This often leads to aggregation of clay particles, and the aggregated clay sheets act as stress-concentration sites in polymer matrix. When the clay sheets exist in such bundles and the original d-space is unaltered in polymer matrix is referred to as a tactoid nanocomposite. If the interlayer spacing of clay sheets is increased and the clay sheets are poorly dispersed, the composite referred to as intercalated nanocomposite. If the clay sheets are well dispersed and distributed, the composite is referred to as exfoliated nanocomposites. [26]

The inorganic ions in the clay can be effectively replaced with organic cationic surfactant molecules through cation- exchange reactions. There are three main causes of cation exchange capacity of the clay minerals;

- Unsatisfied charges which can be balanced by adsorbed cations would be created by broken bonds near the edges of the silica alumina units. Thus the cation exchange capacity would increase as the number of broken bonds increases and the particle size decreases. The exchangeable cations are held around the edges of the flakes.
- Substitution within the lattice of trivalent aluminum for quadrivalent silicon in the tetrahedral sheet and lower valence of ions, particularly magnesium, for trivalent aluminum in the octahedral sheet result in unbalanced charges in the structural units of some of the clay minerals. In montmorillonite and vermiculite substitutions within the lattice cause about 80% of the total cation exchange capacity. The cations are held mostly on the basal plane surfaces.
- The hydrogen of exposed hydroxyl groups would be replaced by cationic exchange.

The results in the expansion of the interlayer spacing, which leads to an increase in the basal spacing, is shown in Figure 2.11.

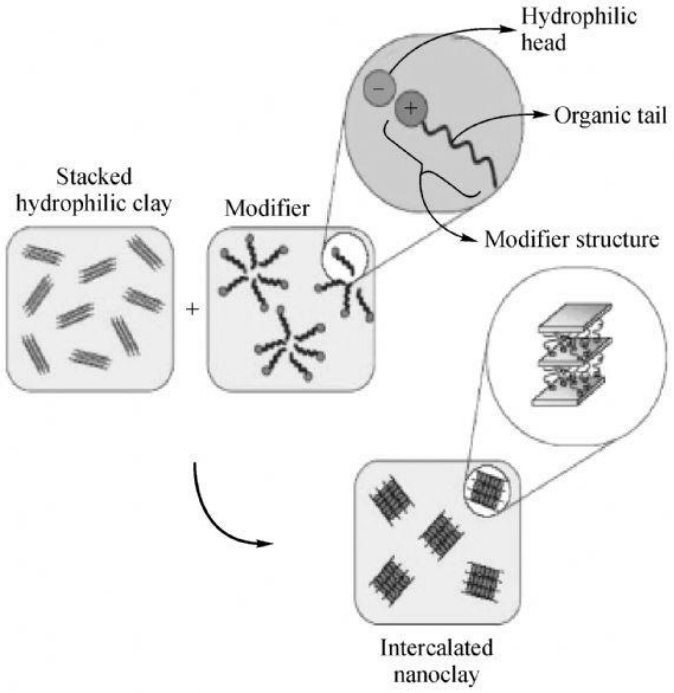

Figure 2. 11 Clay modification process [26]

To prepare superhydrophobic surfaces; 20g of the silica and 50g of the MMT particles were dissolved in 350ml and 250 ml Hexane, respectively. The solutions were mixed by mechanical mixer to obtain uniform dispersion for three hours. At the same time, surfactants are dispersed for modification process. Both 6.4 ml FDTS and 6.4 ml OSTM were dissolved in 200 ml hexane by ultrasonic bath and mechanical stirrer. Half of the first two solutions, MMT and silica, were mixed with other half of the surfactant solutions, FDTS and OSTM. Both solutions were stirred during 6 hours at room temperature. After the reaction had completed, solutions were centrifuged at 3000 rpm for 30min by Hettich rotofix 32A centrifugal machine. The modified MMT and silica suspensions were washed repeatedly by distilled water, then filtrated until no precipitate appeared. Before drying, vacuum oven was heated 150˚C and pumped several times to clean. The filtrated cakes were dried in vacuum oven at 75˚C for 18 hours. Agate mortar was used to obtain fine particle size powder.

For anticorrosive purpose; to modify 3 gr silica with 0,01g BTA and 0,01g TTA, the same procedure was applied in 5cc IPA.

2.2.1.5 XRD Analysis

Each of the materials has its own characteristic unit cell parameters such as d-spacing and with Bragg's Law, the value of 'd' can be found easily. Value of d- spacing for MMT particles was measured by XRD equipment in Erciyes University Technology Research Center, Figure 2.12. It is known that, d-space increases with intercalation of inhibitors. After modification, d-space of modified MMT particles with FDTS and OTMS was also measured. The results are shown Figure 2.13 and Figure 2.14, respectively. If d-space increases, θ value must be shifted to the left side. And Bragg's Law shows it to us because λ is constant in the equation. According to the results, pick of MMT particles was shifted from around 7˚ to around 6˚ after modification process.

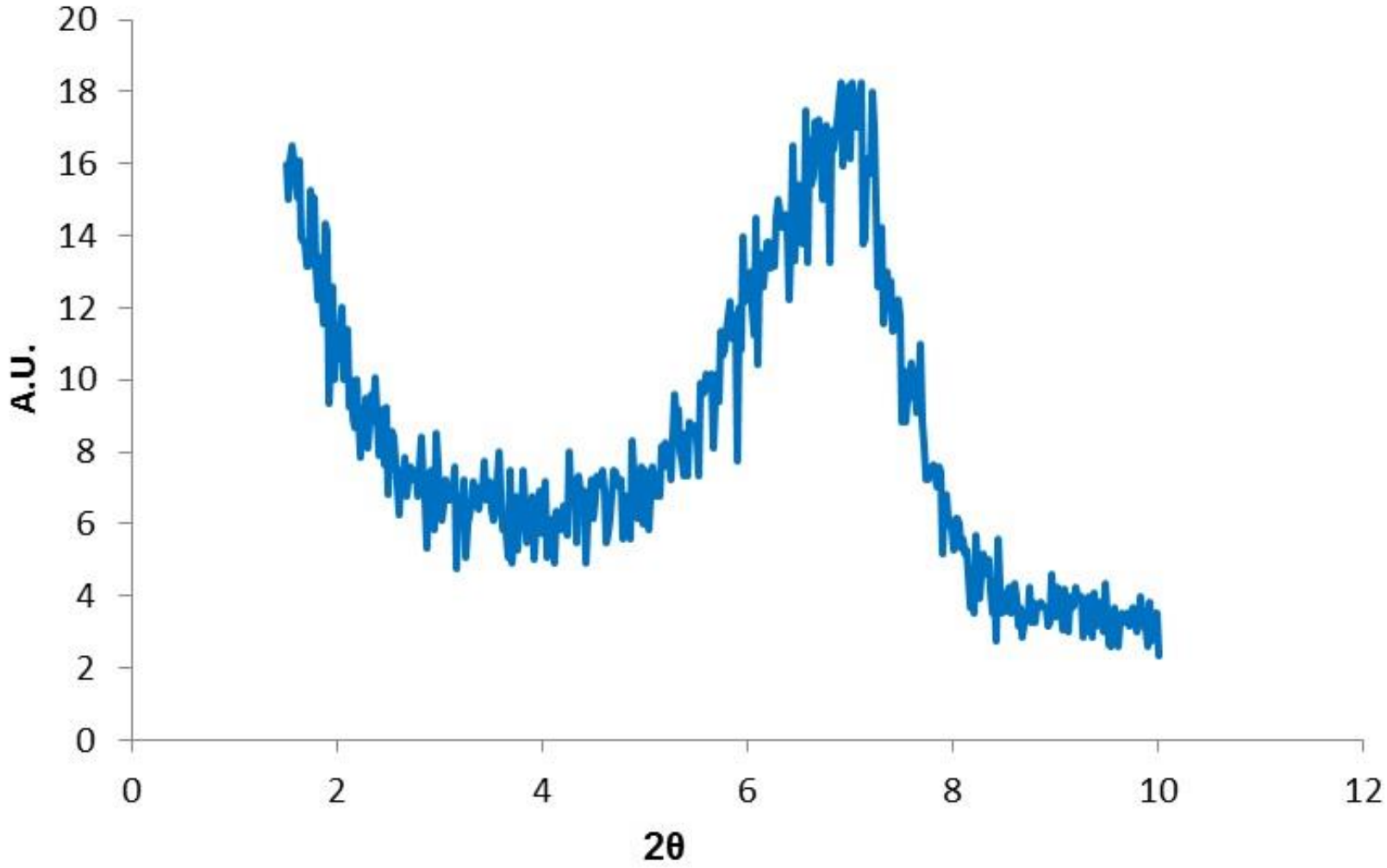

Figure 2. 12 XRD analysis of MMT particles

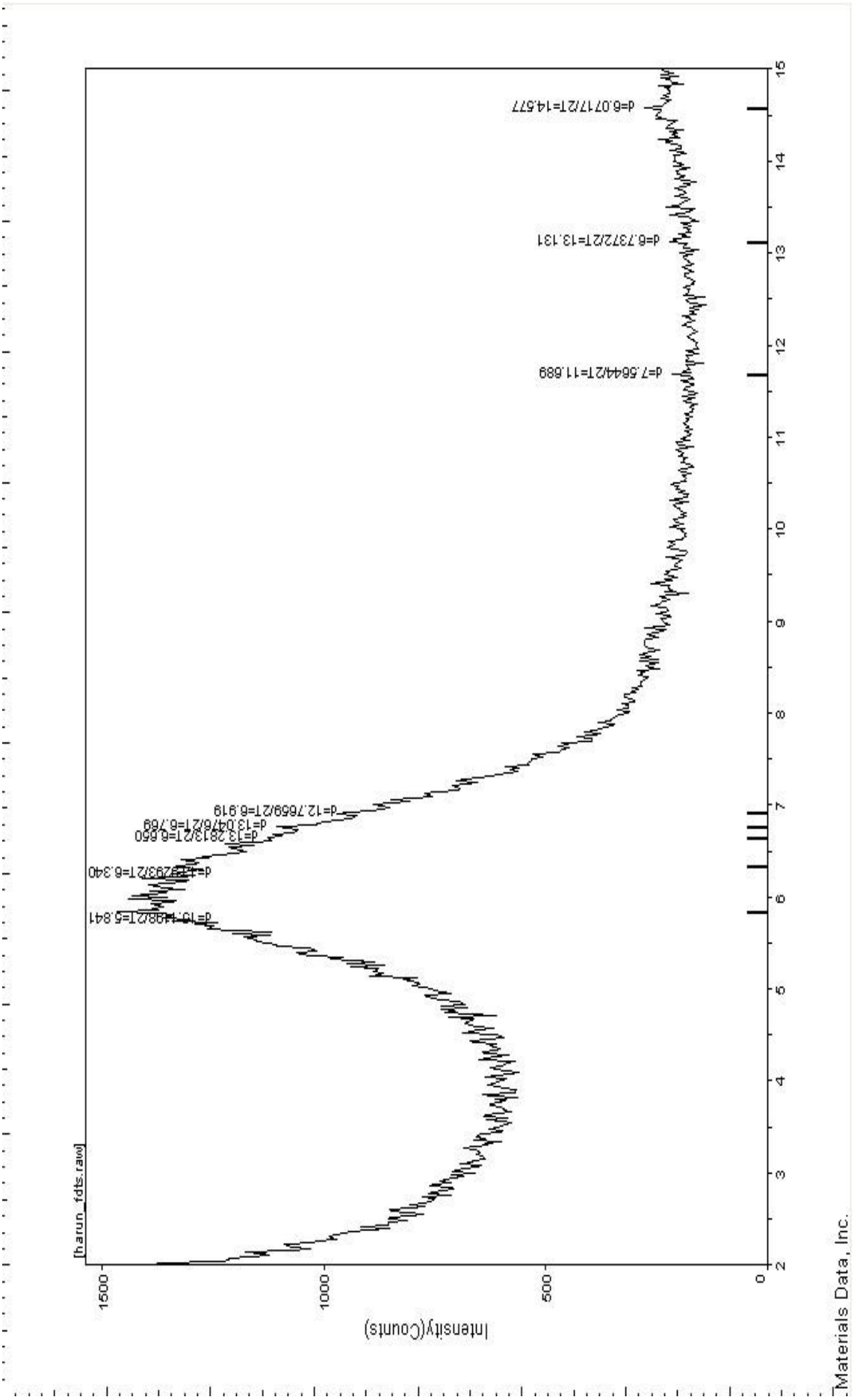

Figure 2. 13 d-spacing of modified MMT particles by Perfluorodecyltrichlorosilane,FDTS

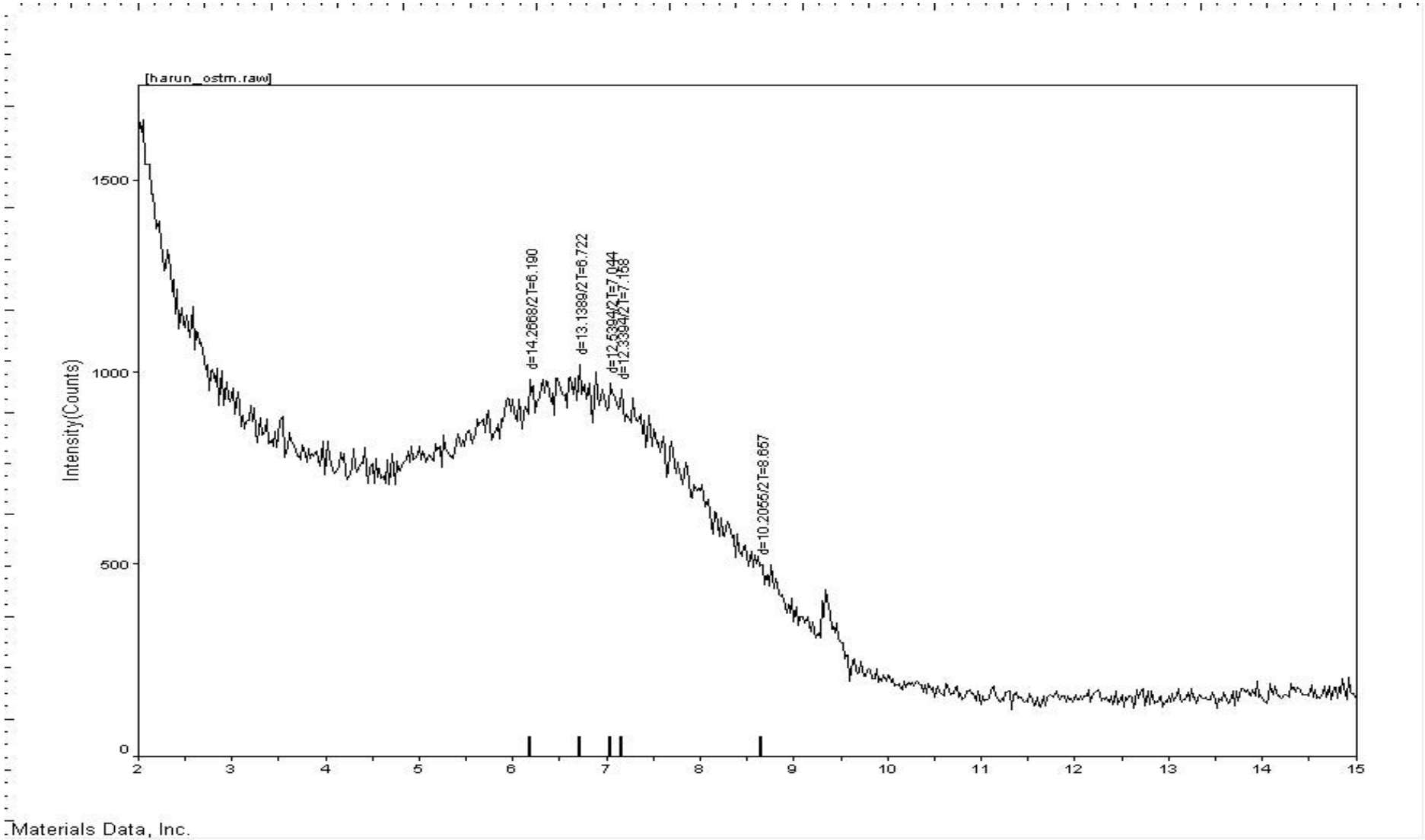

Figure 2. 14 d-spacing of modified MMT particles by OTMS, Octadecyltrimethoxysilane

2.2.2 Applying Nanocomposite Coatings for Superhydrophobic Purpose

2.2.2.1 Matrix Materials

As mentioned in the previous section, there are seven polymer resins which were chosen because of their Si based structure, polarity, viscosity and adhesion ability. First of all, contact angle of glass substrate was measured then substrates were coated with pure matrix materials. All of the samples were coated by spray gun with constant parameters such as distance between gun and sample, and angle of sample.

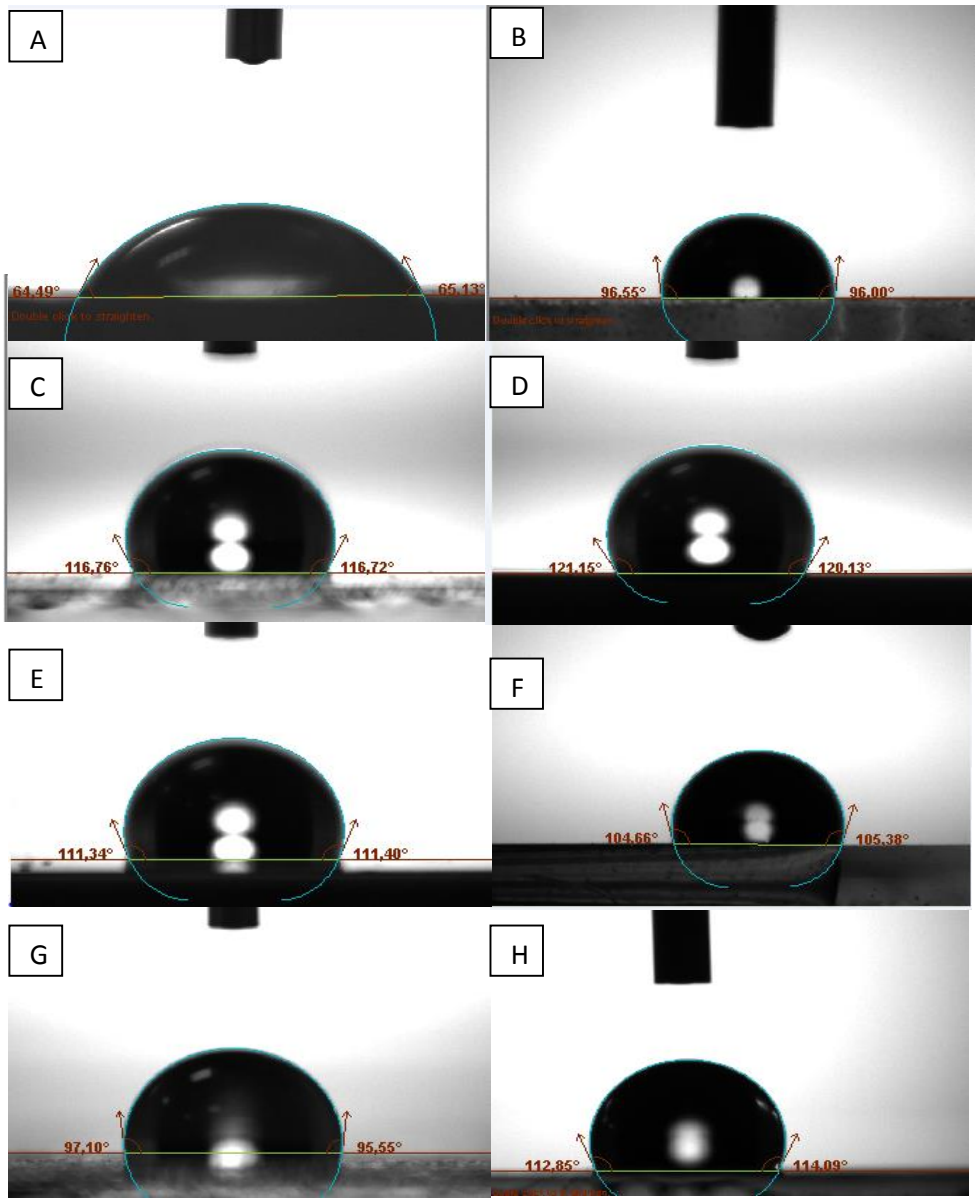

Figure 2. 15 Contact angles of glass samples and pure matrix polymers. A. glass samples without polymer coating, B. Hardsil AM polymer C.1965 polymer, D. 9189 polymer, E. 9187 polymer, F.2577 polymer, G.2620 polymer, H. 1953 polymer

Contact angles of all coated surface were measured by KSV Attention theta light optic goniometer. As it is shown in Figure 2.15, contact angles of pure matrix polymers were also measured and results of contact angles of pure glass samples and matrix polymers (Hardsil AM, 1965, 9189, 9187, 2577, 2620, 19653) are 65˚, 96˚, 116˚, 120˚, 111˚, 104˚, 96˚ and 113˚, respectively.

The results of polymers' contact angles give information about their surface energy. According to surface thermodynamics, materials which have low surface energy, have to give higher value of contact angle, so the higher value of contact angle is, the more hydrophobicity is. If the value of contact angle is not enough to be hydrophobic, hydrophilic matrix will not mix with hydrophobic particles. Although results of all polymers have higher contact angle, some of contact angles of polymers such as 9187 and 9189, decrease by time, Figure 2.16.

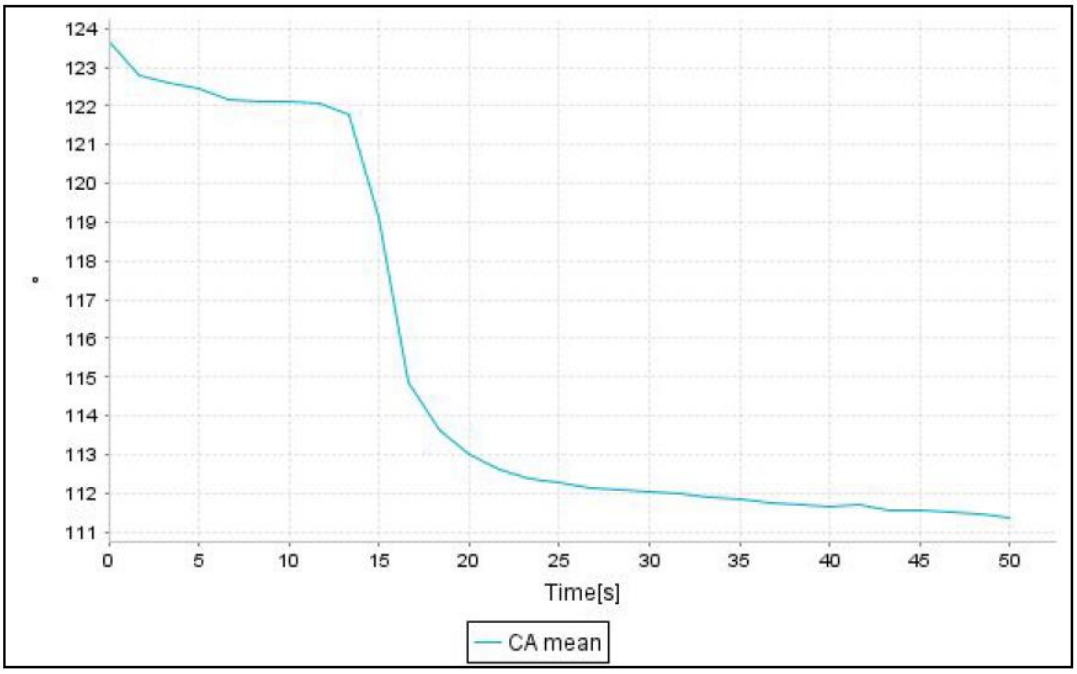

Figure 2. 16 Contact angles vs. time graph of 9187 polymer.

It is expected that, composite materials which are doped with modified silica particles, must have better contact angles than doped with MMT particles. Because silica particles which are stayed on surface of composite, make up nanosize roughness and low surface energy. However some polymers gave better result, others do not mix with silica particles, homogenously. And silica particles could not reach to surface in the polymer

matrix. Because of these reasons, there is no change in surface angle of composite polymer.

According to all these results, three polymer resins were chosen for the following experiments: 2620, 1953 and Hardsil AM.

2.2.2.2 Concentration

The matrix and modified particles with different ratio were vortex mixed for 1 hour. After curing, contact angle of each coated surfaces was measured, and then scratching and brushing tests were applied. Some contact angles results are shown in below. Hardsil AM with MMT particles in different concentration is shown in Figure 2.17 and also Hardsil AM with silica partciles in different concentration is shown in Figure 2.18. As shown in results, nanocomposite with silica particles gave better result than MMT for contact angle, is also shown in Figure 2.19.

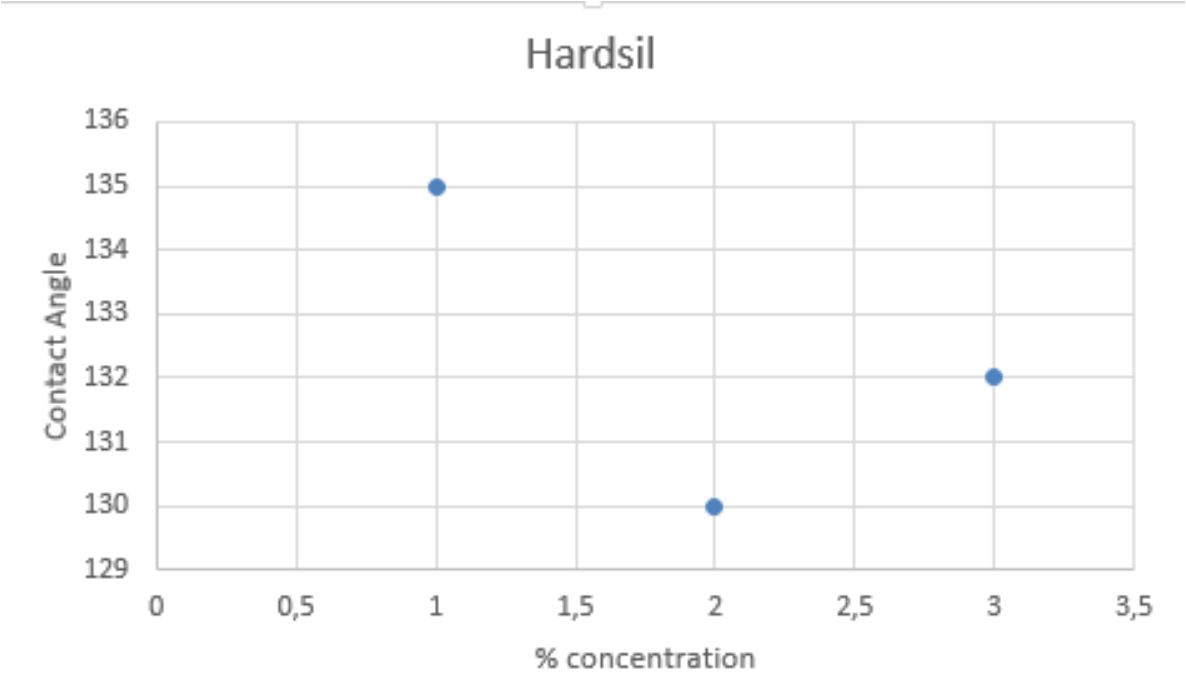

Figure 2. 17 Concentration of modified MMT with 35% Hardsil AM

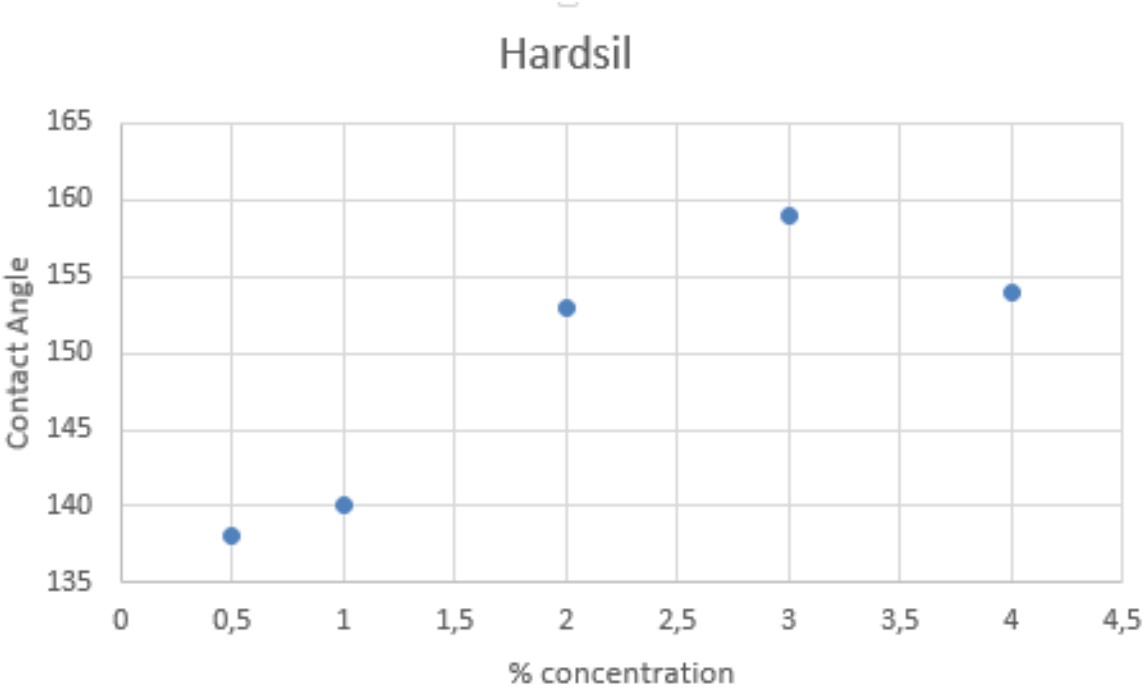

Figure 2. 18 Concentration of Modified Silica with 35% Hardsil AM

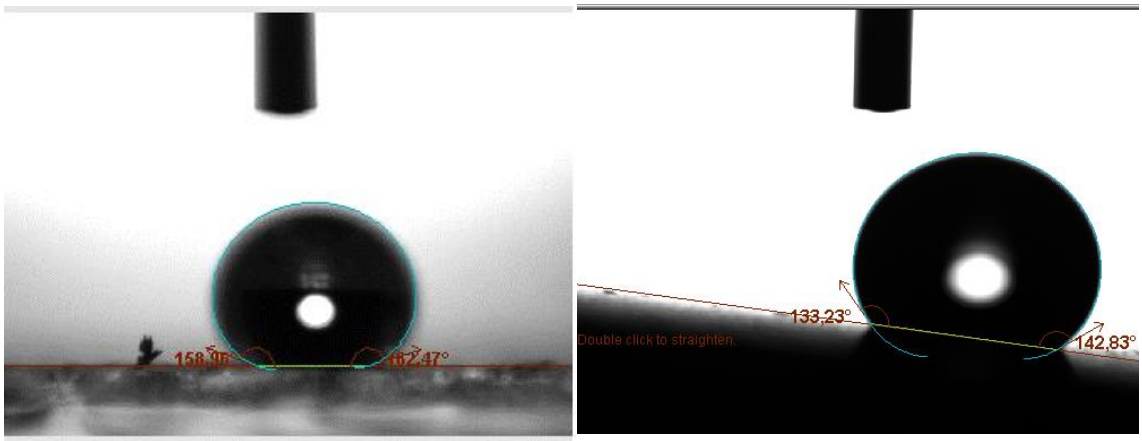

Figure 2. 19 Contact Angles and Contact Angles Hysteresis of 3% Modified Silica with 35% Hardsil AM

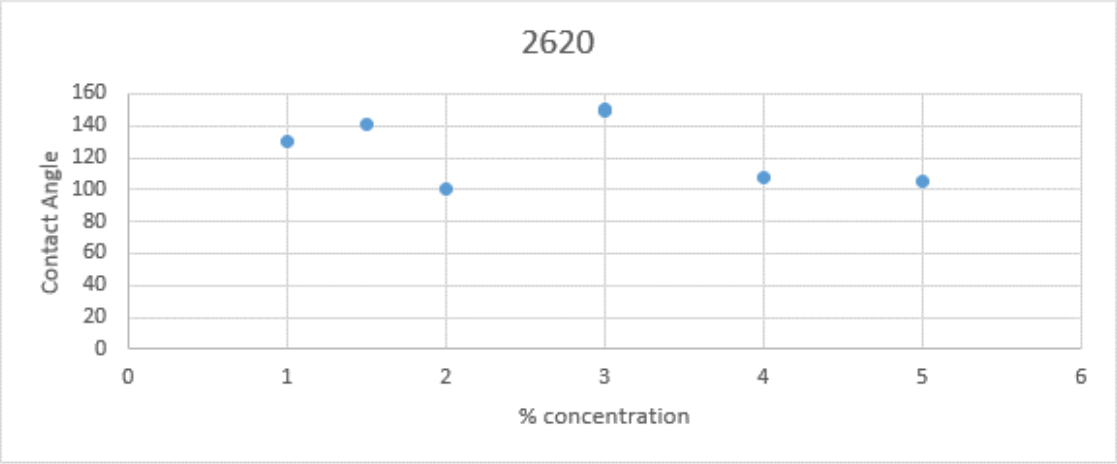

Figure 2. 20 Concentration of 2620 with 2% modified Silica

It is shown in Figure 2.20, contact angles of composite decrease below and above of 3% wt 2620 concentration. When concentration is increased more than 6-7, contact angles decrease to same value of pure 2620 coating. It means that, silica particles cannot find any way for reaching to surface in polymeric structure at more concentration.

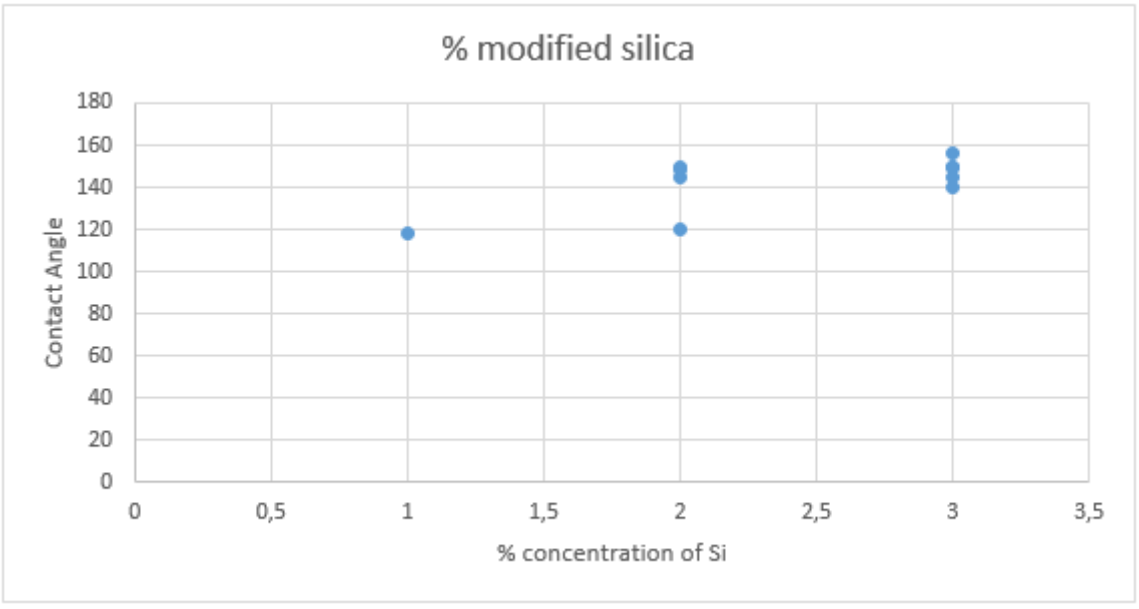

Figure 2. 21 Concentration of modified with 3% for 2620 resin.

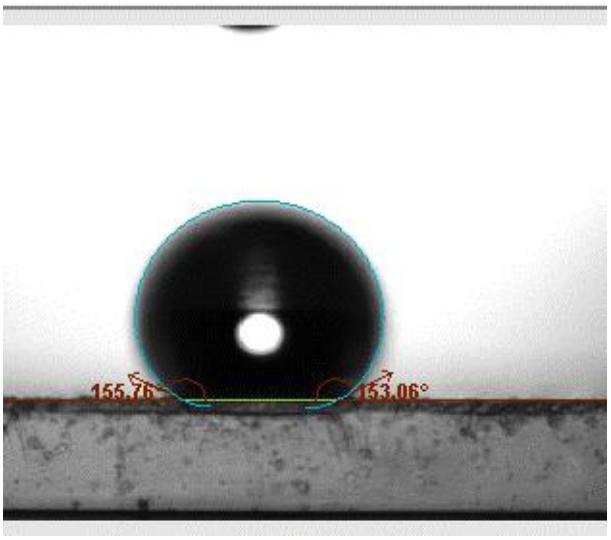

Figure 2. 22 Contact angle of 3% 2620 with 3% modified Silica

The other concentration experiment is made to find optimum values of concentration of modified silica, Figure 2.21. All experiments were made with 3% wt concentration of 2620. As it is seen that, repeatability and values of contact angles are more effective at %3 wt concentration for modified silica in 3% 2620 polymeric matrix. Contact angle measurement of such concentration is shown in Figure 2.22. (Remaining percent of solutions was IPA and it was vaporized at curing period).

There is same experimental result which was repeated for Dow Corn. 1953 resin, Figure 2.23.

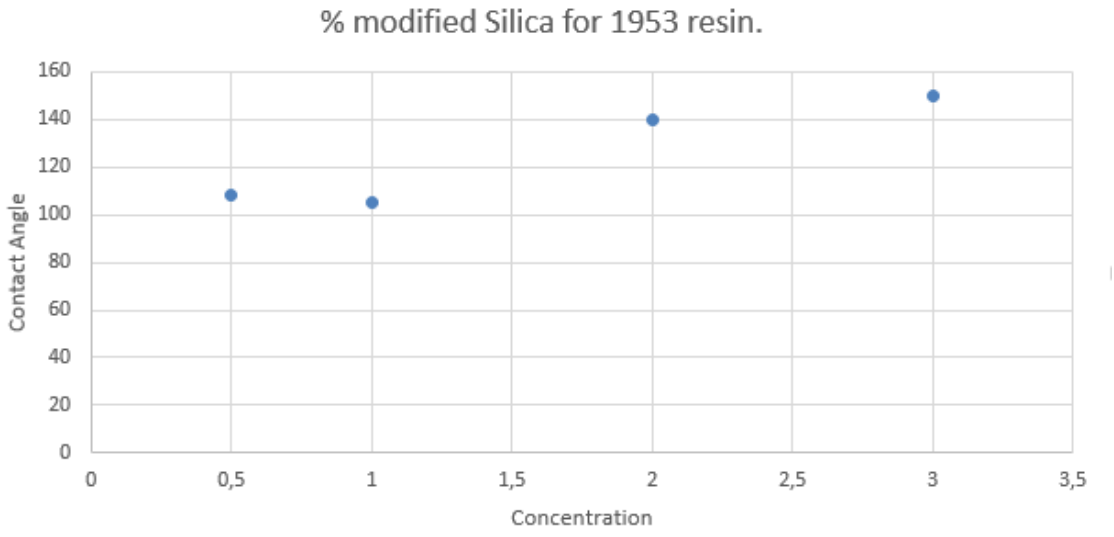

Figure 2. 23 Concentration of modified silica for 1953 resin.

2.2.2.3 Mechanical Properties of Nanocomposites

Adhesion and hardness properties of matrix polymers were controlled by scratching and brushing tests at different times, t. t1: just after curing process, t2: after 30 min, t3: after 24 hours and t4: after 1 months. Hardsil AM has not any problem about adhesion and hardness, however the others can scratch easily with hand, and it is shown Figure 2.24.

Figure 2. 24 After scratching and brushing test

Abrasion test of Hardsil AM polymer was measured by Taber Abrasion Resistance Machine, it is shown on figure 2.25. This technique measures how much material has been removed by abrasion, and is usually reported in milligrams.

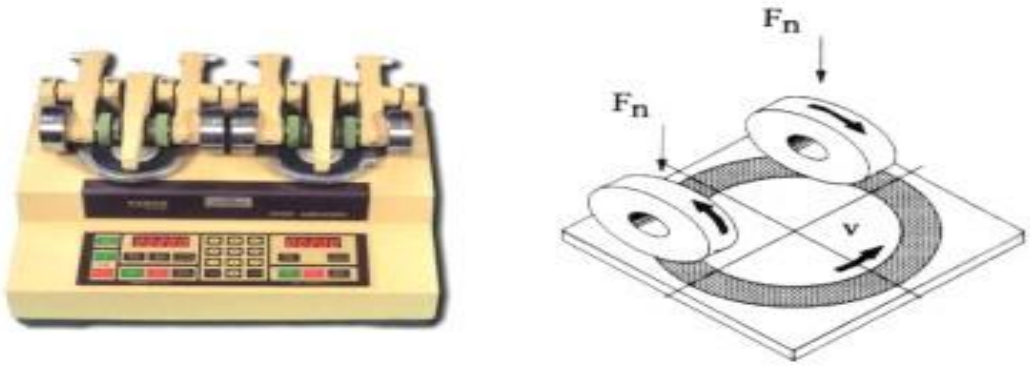

Figure 2. 25 Taber abrasion resistance machine and working principle

All test samples which were prepared for coating, were designed on SolidWorks. And it is shown in Figure 2.26.

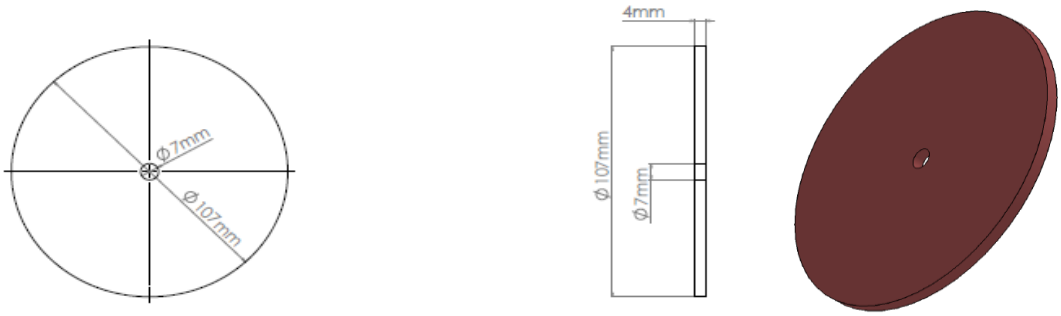

Figure 2. 26 Designed Sample for abrasion test

Nanocomposites were coated on samples and abrasion test applied with CS-10 wheel and 250g load. 500 cycles was applied under %50 vacuum and 72 rad./s speed. The pictures of before and after tests are shown in Figure 2.27.

The number of cycles required to reach a predetermined end point, or the appearance or condition of the specimen after a fixed number of cycles. The evaluation criteria may include: loss in breaking strength, yarn breakage, loss in coating, change in gloss, color loss, or other changes in appearance. In these cases, the abraded sample is usually compared to a known standard of the material tested. When visually inspecting changes in specimen appearance, evaluations should be made using an agreed upon rating system such as a visual grading scale or pass/fail criteria.

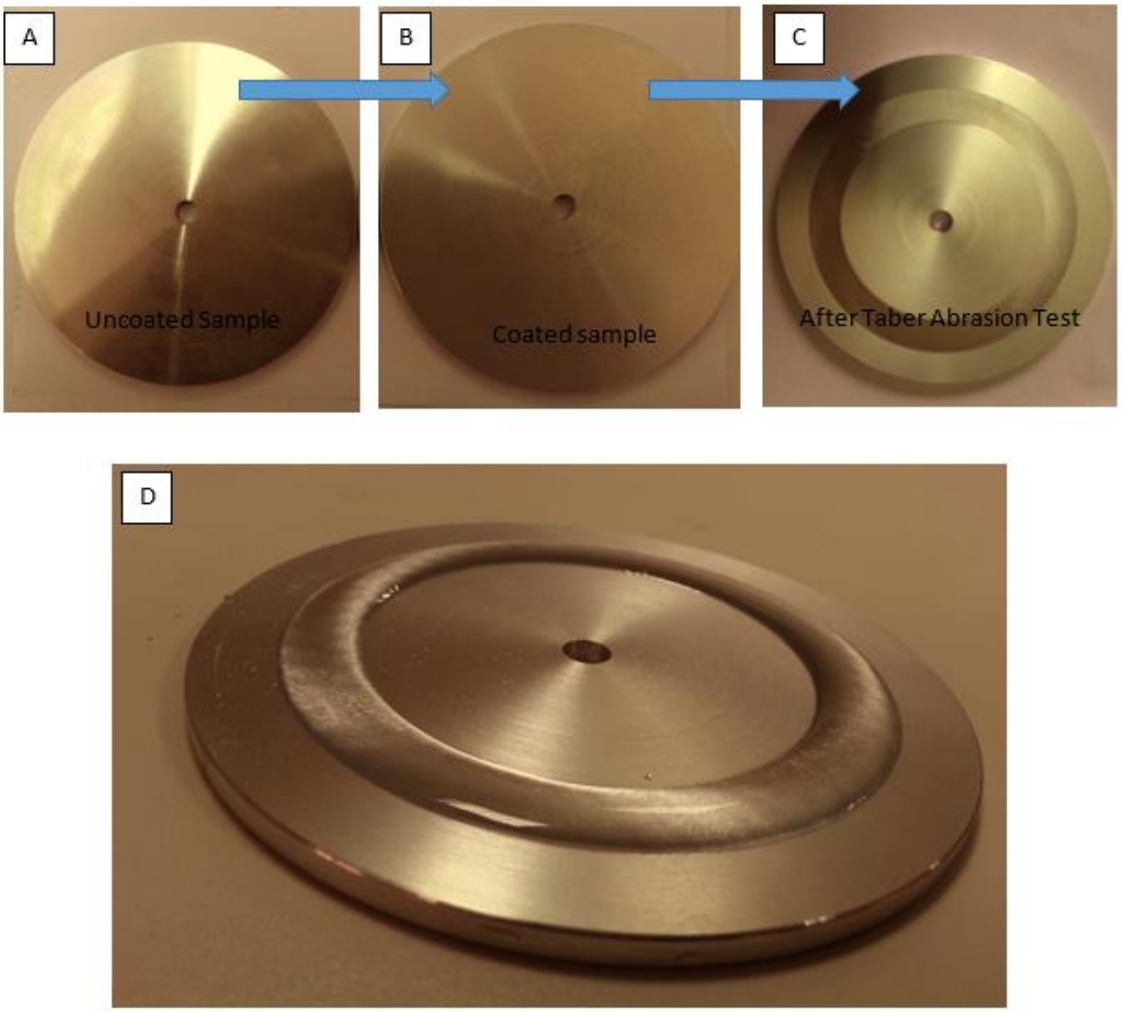

Figure 2. 27 Before and after than abrasion test; A. aluminyum sample, B. Nanocomposite film coated sample, C. After applied abrasion test under 500g, 75 rad/s, and 500 cycles. D. Effects of hydropophicity after abrasion test

Results of Taber Abrasion Test of two different samples which are applied at the same condition, are shown in Table 2.2. Two samples were coated with same composition of nanocomposite.

	Weight of Sample (mg)	Weight of coated Sample(mg)	Weight of coating (mg)	Weight of coated sample after test (mg)	Loss in weight (mg)
Sample 1	1012677	1012903	226	1012806	97
Sample 2	1008725	1008955	230	1008891	64

Table 2. 2 Result of Taber Abrasion Test

2.2.2.4 SEM Results of Nanocomposites

The structure of the nanocomposites were examined using SEM. There are also some impurities which were occurred during spraying process. Results of SEM analysis are shown in figure 2.28, 2.29, and 2.30 with 5000, 30000 and 100000 X magnification.

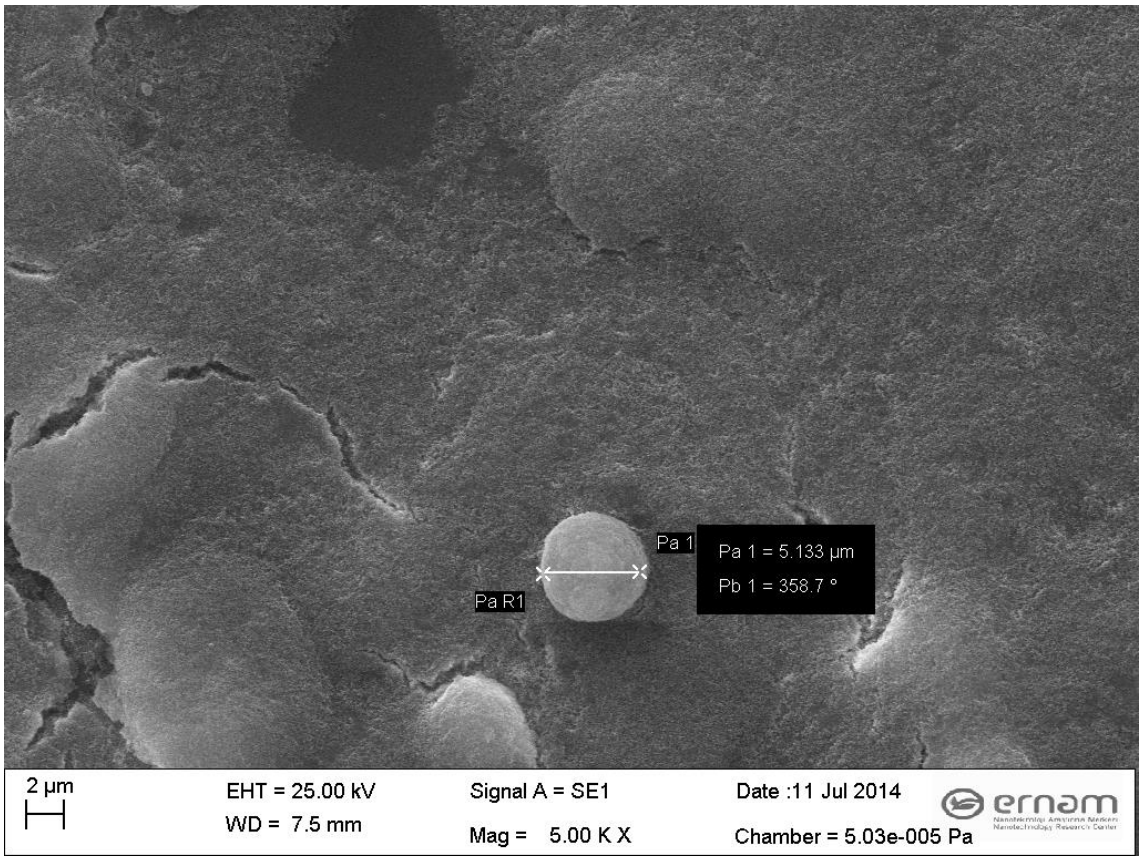

Figure 2. 28 SEM pictures of nanocomposite coating with 5000x

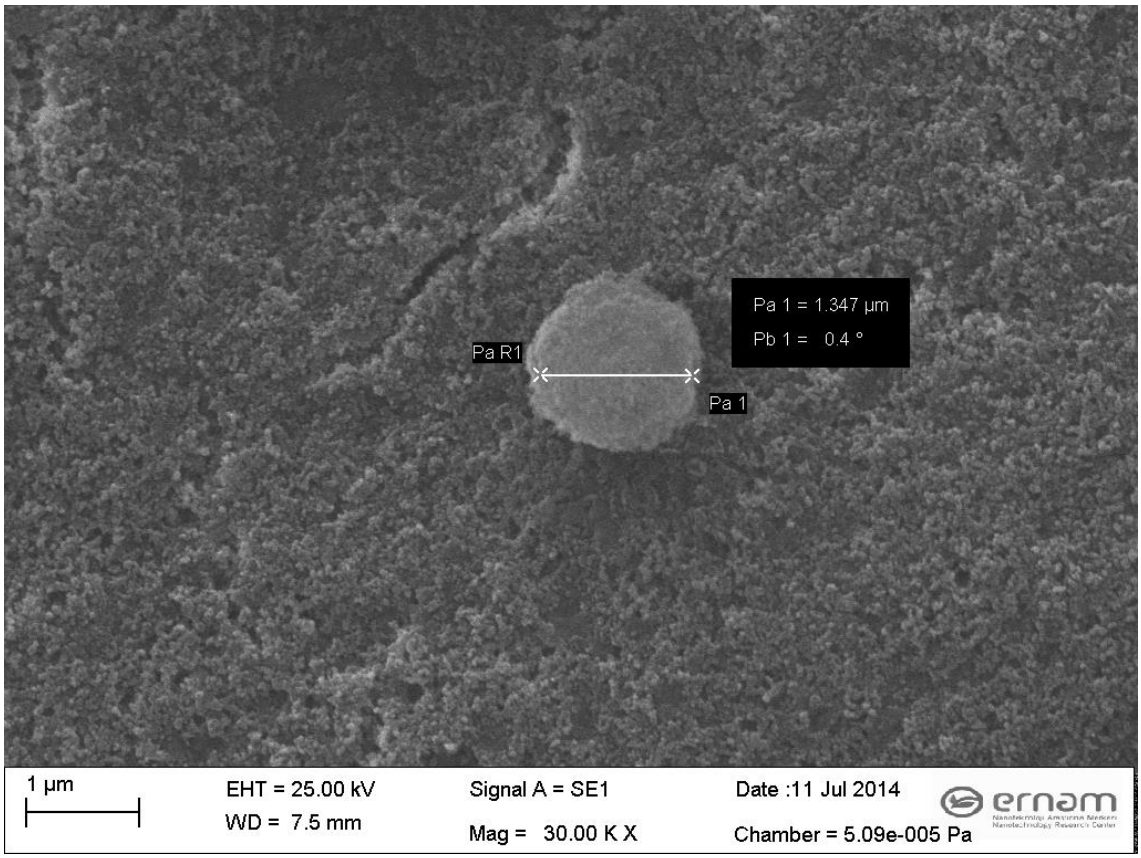

Figure 2. 29 SEM pictures of nanocomposite coating with 30000x

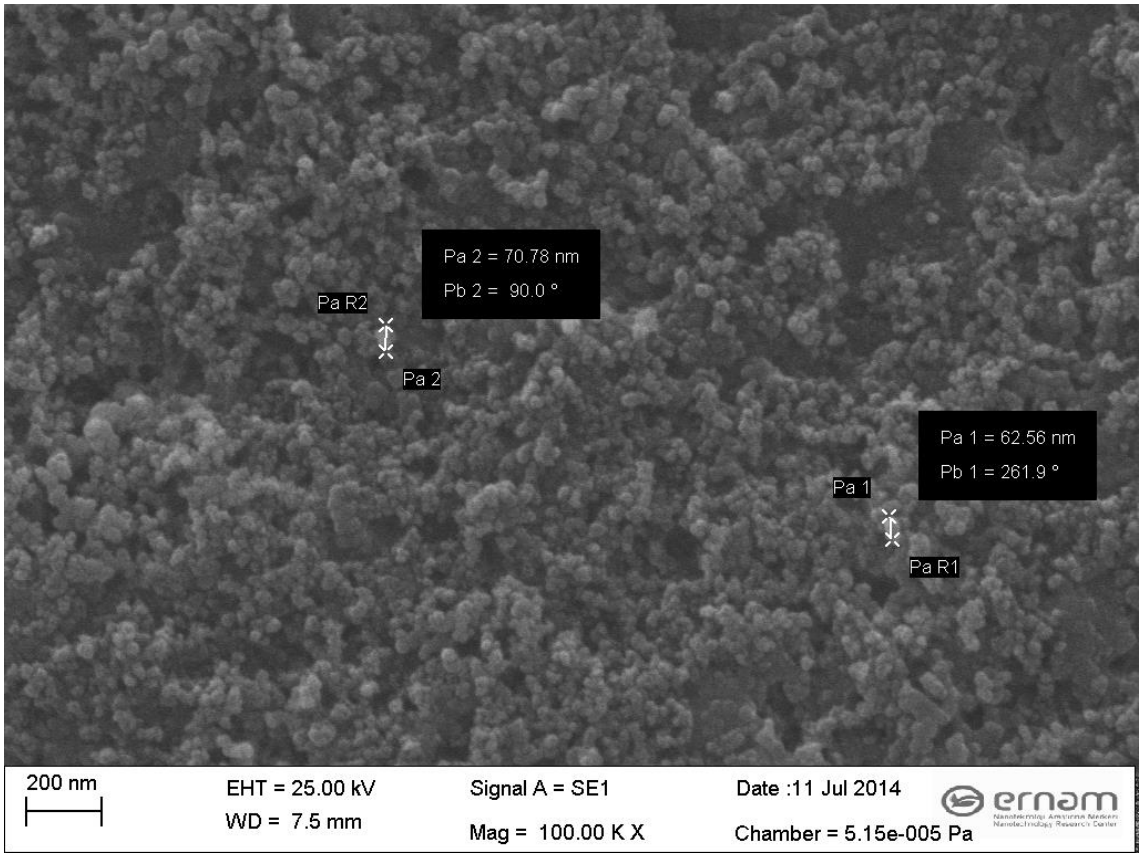

Figure 2. 30 SEM pictures of nanocomposite coating with 100000x

2.2.3 Applying Nanocomposite Coatings for Anti-Corrosion Purpose

It is well known that a better understanding of the relation between the adsorption of surfactant molecules onto metal surface and corrosion inhibition is of great importance for both theoretical and experimental reasons. To neutralize the corrosion, inhibitors should be injected constantly through the system. [27]

Corrosion inhibition has a complex mechanism and depends on the formation of mono - or multi - dimensional protective layers on the metal surface. The protective nature of the surface layer depends on many factors; interaction between inhibitors and matrix materials, incorporation of the inhibitors in the matrix, chemical reactions, etc. The first stage in the action mechanism of the surfactants as corrosion inhibitors in aggressive media is adsorption of the surfactants molecules on the particles. Corrosion inhibition depends on the adsorption ability of the surfactant molecules on the corroding surface, which is directly related to the capacity of the surfactant to aggregate to form clusters (micelles). The critical micelle concentration, CMC, is a key factor in determining the effectiveness of a corrosion inhibitor. Below CMC, the molecules tend to aggregate at the interface, and this interfacial aggregation reduces the surface tension. Above CMC, the metal surface is covered with a monolayer of surfactant molecules and the additional molecules combine to form micelles or multiple layers.

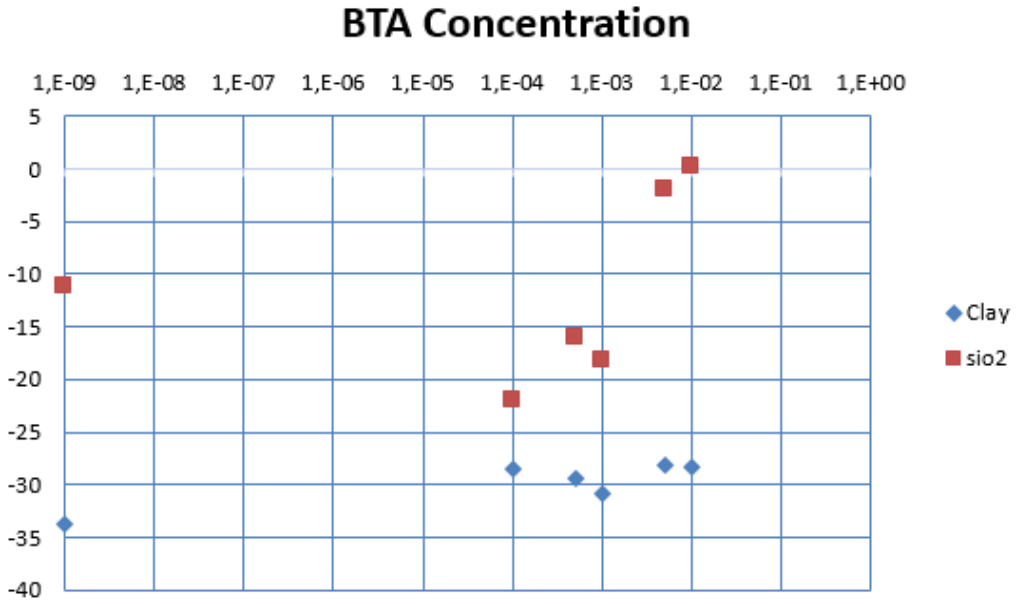

Figure 2. 31 Zeta potential of silica and clay particles according to BTA concentration

As said in previous section, silica and clay particles were modified with same process. Before modification process to understand of CMC, zeta potential of silica and clay particles were measured according to different inhibitor concentrations, in Figure 2.31.

To understand of effects of corrosion inhibitors were tested at 85/85 (85 ˚C temperature and %85 humidity) during three days in environmental tasting cabined. Copper samples with modified silica particles' pictures which are taken after and before tests, were shown in Figure 2.32.

Hardsil AM matrix is also used for nanocomposite coatings for anti-corrosive purpose. Pictures of control sample, Hardsil AM polymer, reinforced with BTA and TTA modified silica particles nanocomposites are taken after 85/85 testing during three days. All results are also shown in Figure 2.33. There is no corrosion on pure matrix but it just protects to the surface area which coated. Nanocomposites protect more surface area than it coated, because of gas releasing. And also, it is clearly seen that, BTA modified particles gave better result than TTA modified particles.

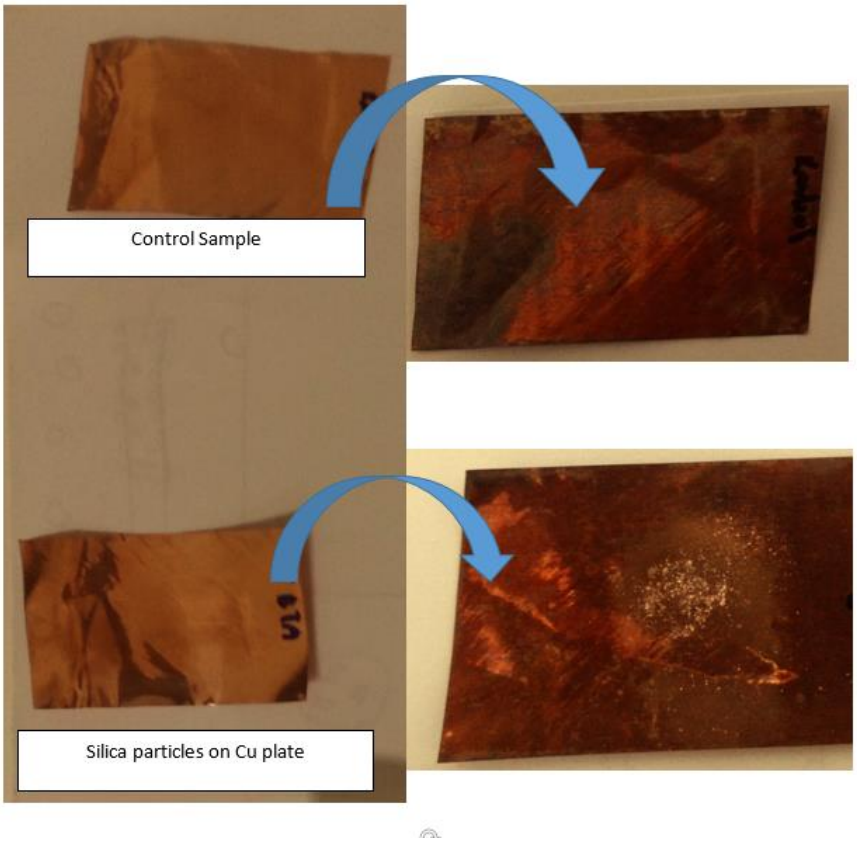

Figure 2. 32 Before and after than testing of modified silica particles

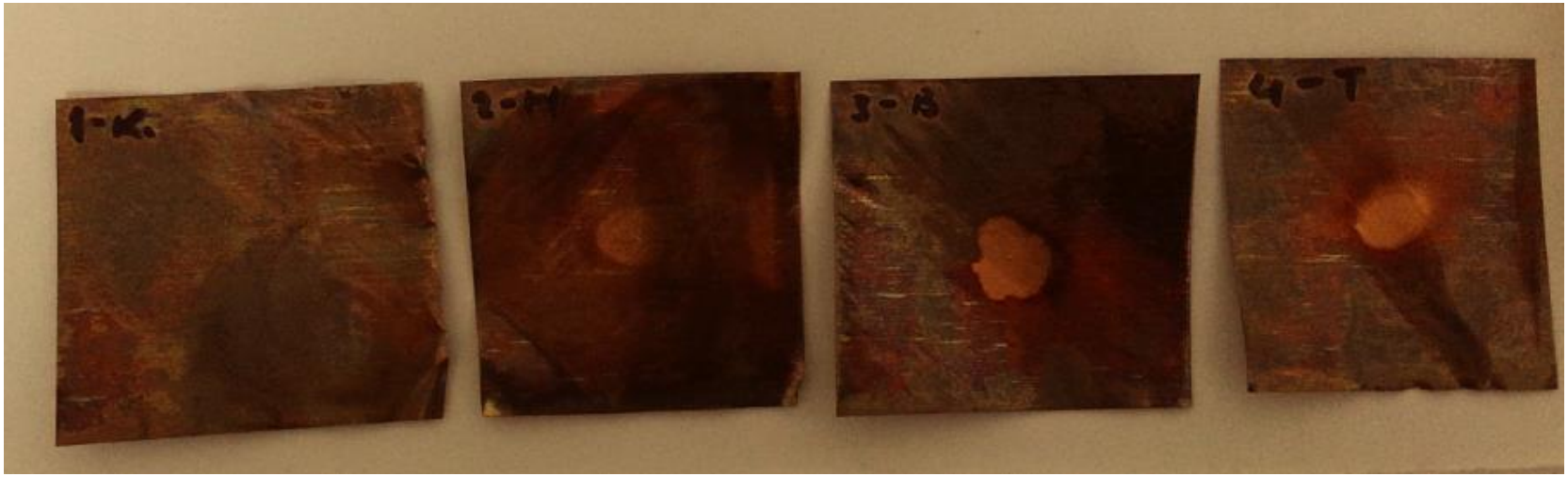

Figure 2. 33 After than three days 85/85 test, 1-K; control sample, 2-H; Hardsil AM polymer resin, 3-B; BTA doped particles reinforced nanocomposite, 4-T; TTA doped particles reinforced nanocomposite

CHAPTER 3

CONCLUSION

The results showed that several parameters such as particle size, type of matrix materials, and type of modification agents affect superhydrophobicity. Surface roughness of nanocomposite coating materials is changed by particle size, as discussed in chapter 3. However, modified particles did not mixed with most of the polymer. Because mechanism of mixing process depends on the polarity of both matrix polymer and reinforced materials.

As seen in the results, doped Hardsil AM polymer with FDTS modified silica particles gave the best result in contact angle and adhesion, thanks to their characteristic structure and polarity. Silica particles mixed homogenously and separated into inside and surface of coating materials. Superhydrophobicity of the nanocomposite was supported by two mechanisms, one of them is low surface energy of modified silica particles which stayed at surface and the second one is surface roughness which is created by same particles. After experiments, CA of composite coating reached more than 175˚ with %2-3 wt concentrated nanocomposite and droplets was bouncing and rolling on surface, as shown in Figure 3.1.

Figure 3 1 Bounced and rolled water droplets on superhydrophobic surface

As mentioned in previous works of researchers, superhydrophobic surface can be used for anti-icing purpose. Coated surfaces were waited at -20 ˚C during two days in climate cabined and there was no ice formation.

For anti-corrosive aim, BTA modified silica particles gave better result. One of the most important parameter for resistivity of corrosion is structure of matrix materials. Because it effects gas realizing of corrosion inhibitors and creating of protective layer above the surface. If structure of matrix polymer is close packed, protective layers stay surface at long time but cannot protect wide area. If it is not, protective layers will not stay at surface during long time but it can protect more area and also layer can be created easily.

REFERENCES

[1] C.-Y. Hui and A. Jagota, "Surface Tension, Surface Energy, and Chemical Potential Due to Their Difference", Langmuir, Vol. 29, pp. 11310-11316, 2013.

[2] B. Lautrup, Physics of Continuous Matter, CRC Press, Boca Raton, 2011.

[3] R. Shuttleworth, "The Surface Tension of Solids", Proc. Phys. Soc. A, Vol. 63, No. 5, pp. 444-457, 1950.

[4] Slip and Leveling Agent, 2010, http://www.afcona.com.my/Slip_and_Leveling_agent_mar_2010.pdf

[5] E. M. de C. Lobato, Determination of Surface Free Energies and Aspec Ratio of Talc, M.S. Thesis, Virginia Polytechnic Institute and State University, 2004.

[6] Surface Energy, http://en.wikipedia.org/wiki/Surface_energy

[7] Chapter 7. Surface Thermodynamics, http://www.most.gov.mm/techuni/media/ChT03013_26.pdf

[8] Surface Tension, http://scipp.ucsc.edu/~haber/ph5B/bubble.pdf

[9] Ionic Bonding, http://en.wikipedia.org/wiki/Ionic_bonding

[10] S.S. Latthe, A.B. Gurav, C. S. Maruti, and R. S. Vhatkar, "Recent Progress In Preparation of Superhydrophobic Surfaces: A Review", Journal of Surface Engineered Materials and Advanced Technology, Vol. 2, pp. 76-94, 2012.

[11] M. Ma, and R. M. Hill, "Superhydrophobic Surfaces", Current Opinion in Colloid & Interface Science., Vol. 11, pp. 193-202, 2006.

[12] W. A. Daoud, Self-Cleaning Materials and Surfaces, Wiley, New Delhi, 2013.

[13] O. Nimittrakoolchai, S. Supothina, “Deposition of Organic - Based Superhydrophobic Films for Anti-Adhesion and Self-Cleaning Applications”, Journal of the European Ceramic Society, Vol. 28, pp. 947-952, 2008.

[14] X. Li, D. Reinhoudt, and M. C. Calama, “What do we need for a superhydrophobic surface? A review on the recent progress in the preparation of superhydrophobic surfaces”, Chem. Soc. Rev., Vol. 36, pp. 1350-1368, 2007.

[15] H. M. Shang, Y. Wang, S. J. Limmer, T. P. Chou, K. Takahashi, and G. Z. Cao, “Optically Transparent Superhydrophobic Silica-Based Films”, Thin Solid Films, Vol. 472, pp. 37-43, 2005.

[16] S. A. Kulinich, and M. Farzaneh, “Ice Adhesion on Super-hydrophobic Surfaces”, Applied Surface Science, Vol. 255, pp. 8153-8157, 2009.

[17] A. J. Meuler, J. D. Smith, K. K. Varanasi, J. M. Mabry, G. H. McKinley, and R. E. Cohen, “Relationships Between Water Wettability and Ice Adhesion”, Vol. 2, No. 11, 2010.

[18] D. P. Subedi, “Contact Angle Measurement for the Surface Characterization of Solids”, the Himalayan Physics, Vol. 2, 2011.

[19] Y. Yuan, and T. R. Lee, Contact Angle and Wetting Properties, Springer Berlin Heidelberg, Houston, 2013.

[20] D. O. Njobuenwu, E. O. Oboho, and R. H. Gumus, “Determination of Contact Angle from Contact Area of Liquid Droplet Spreading on Solid Substrate”, Leonardo Electronic Journal of Practices and Technologies, Vol. 10, pp. 29-38, 2007.

[21] W. C. Bigelow, D. L. Pickett, and W. A. Zisman, “Oleophobic Monolayers: I. Films Adsorbed from Solutions in Non-Polar Liquids”, Journal of Colloid Science, Vol. 1, pp. 513-538, 1946.

[22] Goniometer, http://en.wikipedia.org/wiki/Goniometer

[23] A. E. Gomez, R. Majithia, C. Levert, and K. E. Meissner, “Super-wetting, Wafer-Sized Silicon Nonowire Surfaces with Hierarchical Roughness and Low Defects”, RSC Advances, Vol. 2, pp. 11472-11480, 2012.

[24] Bentonite, http://en.wikipedia.org/wiki/Bentonite

[25] B. W. Jo, “Mechanical Properties of Nano-MMT Reinforced Polymer Composite and Polymer Concrete”, Construction and Building Materials, Vol. 22, pp. 14-20, 2008.

[26] K. R. V. Mahesh, H. N. N. Murthy, B. E. Kumaraswamy, N. Raghavendra, R. Sridhar, M. Krishna, N. Pattar, R. Pal, and B. S. Sherigara, “Synthesis and Characterization of Organomodified Na-MMT Using Cation and Anion Surfactants”, Frontiers of Chemistry in China, Vol. 6, pp. 153-158, 2011.

[27] M. A. Malik, M. A. Hashim, F. Nabi, S. A. Thabaiti, and Z. Khan, “Anti-corrosion Ability of Surfactants: A Review”, Int. J. Electrochem. Sci., Vol. 6, pp. 1927-1948, 2011.

[28] D. R. Paul, and L. M. Robeson, “Polymer Nanotechnology: Nanocomposites”, Polymer, Vol. 49, pp. 3187-3204, 2008.

[29] H. Wang, L. Tang, X. Wu, W. Dai, and Y. Qiu, “Fabrication and Anti-Frosting Performance of Super Hydrophobic Coating Based on Modified Nano-Sized Calcium Carbonate and Ordinary Polycrylate”, Applied Surface Science, Vol. 253, pp. 8818-8824, 2007.

[30] M. Nosonovsky, and B. Bhushan, “Biomimetic Superhydrophobic Surfaces: Multiscale Approach”, Nano Letters, Vol. 7, No. 9, pp. 2633-2637, 2007.

[31] L. Feng, S. Li, Y. Li, H. Li, L. Zhang, J. Zhai, Y. Song, B. Liu, L. Jiang, and D. Zhu, “Super-Hydraphobic Surfaces: From Natural to Artificial”, Advanced Materials, Vol.14, No. 24, pp. 1857-1860, 2002.

[32] L. Cao, A. K. Jones, V. K. Sikka, J. Wu, and D. Gao, “Anti-Icing Superhydrophobic Coatings”, Langmuir Letter, Vol. 25, No. 21, pp. 12444-12448, 2009.

[33] E. A. Flood, and G. C. Benson, “Surface Energy and Surface Tension”, Canadian Journal of Chemistry, Vol. 46, pp. 1297-1316, 1968.

[34] J. Xiong, Z. Zheng, H. Jiang, S. Ye, and X. Wang, “Reinforcement of Polyurethane Composites with an Organically Modified Montmorillonite”, Composites: Part A, Vol. 38, pp. 132-137, 2007.

[35] A. Steele, I. Bayer, and E. Loth, “Adhesion Strength and Superhydrophobicity of Polyurethane/Organoclay Nanocomposite Coatings”, Journal of Applied Polymer Science, Vol. 125, pp. E445-E452, 2012.

[36] L. M. Lander, L. M. Siewierski, W. J. Brittain, and E. A. Vogler, “A Systematic Comparsion of Contact Angle Methods”, Langmuir, Vol 9, pp. 2237-2239, 1993.

[37] K. Kabza, J. E. Gestwicki, and J. L. McGrath, “Contact Angle Goniometry as a Tool for Surface Tension Measurements of Solids, Using Zisman Plot Method”, Journal of Chemical Education, Vol. 77, No. 1, pp. 63-65, 2000.

[38] E. L. decker, B. Frank, Y. Suo, and s. Garoff, “Physics of Contact Angle Measurement”, Colloids and Surfaces A: Physicochem. Eng. Aspects. Vol. 156, pp. 177-189, 1999.

[39] Y. S. Lee, Self-Assembly and Nanotechnology Systems, Wiley, New Jersey, 2012.

[40] H. Y. Erbil, Surface Chemistry of Solid and Liquid Interfaces, Wiley, Kocaeli, 2006.

[41] S. E. Builder, Hydrophobic Interaction Chromatography, Amersham Pharmacia Biotech, San Francisco, 1993.

[42] W. Liu, W. T. Zheng, and Q. Jiang, “First-Principles Study of the Surface Energy and Work Function of III-V Semiconductor Compounds”, Physical Review B, Vol 75, pp. 235322(8), 2007.

[43] A. Sklodowska, M. Wozniak, and R. Matlakowska, “The Method of Cantact Angle Measurement and Estimation of Work of Adhesion in Bioleaching of Metals”, Biological Procedures Online, Vol. 1, No. 3, pp. 114-121, 1999.

[44] J. Bravo, L. Zhai, Z. Wu, R. E. Cohen, and M. F. Rubner, “Transparent Superhydrophobic Films Based on Silica Nanoparticles”, Langmuir, Vol. 23, pp. 7293-7298, 2007.

[45] G. Zhang, D. Wang, Z. Gu, and H. Möhwald, “Fabrication of Superhydrophobic Surfaces from Binary Colloidal Assembly”, Langmuir, Vol. 21, pp. 9143-9148, 2005.

[46] H. X. Ren, X. J. Huang, O. Yarimaga, Y.K. Choi, and N. Gu, “A cauliflower-like gold structure for superhydrophobicity”, Journal of Colloid and Interface Science, Vol. 334, pp. 103-107, 2009

[47] Y.H. Yeong, A. Steele, E. Loth, I. Bayer, G. Combarieu at al. “Temperature and humidity effects on superhydrophobicity of nanocomposite coatings”, Applied Physics Letters, Vol. 100, pp. 03112, 2012

[48] W.D. Bascom, R.L. Cottingtom, and C.R. Singleterry, “Ice Adhesion to Hydrophilic and Hydrophobic Surfaces”, The Journal of Adhesion, Vol. 1, pp. 246-263, 1969

[49] P. Manoudis, S. Papadopoulou, I. Karapanagiotis, A. Tsakalof, I.Zuburtikudis and C.Panayiotou, “Polymer – Silica nanoparticles composite films as protective coatings for stone-based monuments”, Journal of Physics: Conference Series Vol. 61, pp. 1361-1365,2007

[50] G.Navascues, “Liquid surfaces: theory of surface tension”, Rep. Prog. Phys., Vol. 42, pp.071131+58, 1979.

[51] B. Bhushan, K. Koch, Y.C. Jung, “Fabrication and characterization of the hierarchical structure for superhydrophobicity and self-cleaning”, Ultramicroscopy, Vol. 109, pp. 10029-10034, 2009.

[52] B. Bhushan, Y.C. Jung, “Contact angle, adhesion and friction properties of micro- and nanopatterned polymers for superhydrophobicity”, Nanotechnology, Vol. 17, pp. 4970-4980, 2006

[53] Z. Burton, B. Bhushan, “Hydrophobicity, Adhesion, and Friction Properties of Nanopatterned Polymers and Scale Dependence for Micro- and Nanoelectromechanical Systems”, NanoLetters, Vol.5, pp. 1607-1613